universität innsbruck

Subradiance in atomic arrays with a V-type level structure

Master Thesis

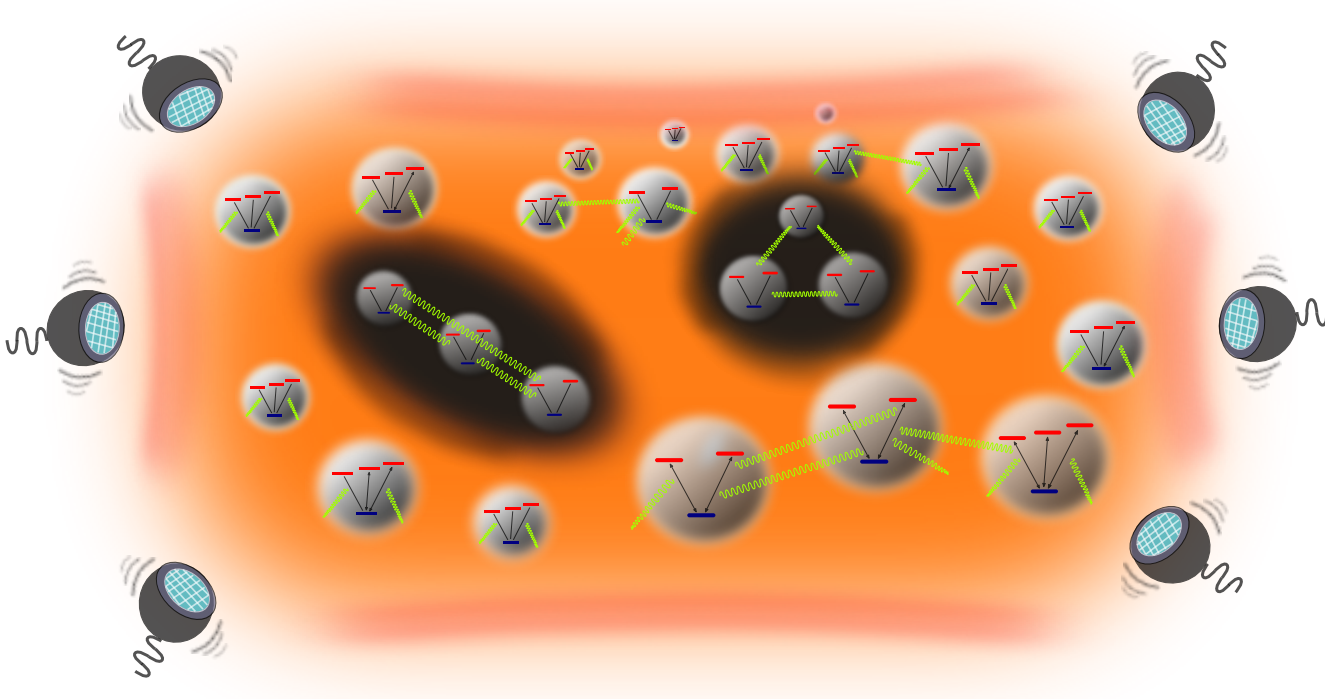

Author:
Raphael Holzinger Bsc.

Supervisor:
Univ.-Prof. Dr. Helmut Ritsch

A thesis submitted in fulfillment of the requirements for the degree of Master of Science

in the

Cavity Quantum Electrodynamics Group,
Institut für Theoretische Physik Innsbruck

January 22, 2019

Abstract

Spontaneous emission in quantum emitters is modified by other atoms nearby, leading to super- and subradiance. We investigate the subradiant behaviour of V-type multilevel emitters in close vicinity to each other. In particular we are interested in collective excited states with more than one excitation. As specific geometric examples we study the equilateral triangle and the linear chain at interatomic distances smaller than the transition wavelength between the atomic states. For the equilateral triangle an analytical treatment is possible for every symmetric configuration. In this setup the Hamiltonian has a maximally entangled, antisymmetric doubly excited eigenstate involving the superpositions of all three atoms, which shows subradiance as opposed to superradiance. In the ideal case the dark state decouples completely from the vacuum radiation field and therefore does not decay spontaneously. Numerical simulations involving different dipole orientations and interatomic distances are presented and their subradiant behaviour is investigated.

Zusammenfassung

In dieser Arbeit demonstrieren wir die subradianten Eigenschaften von V-artigen mehrstufigen Emittern in geringem Abstand zueinander, mit dem gleichseitigen Dreieck and der linearen Kette bei atomaren Abständen kleiner als die Übergangswellenlänge λ_0, als spezifische Beispiele.
Für das gleichseitige Dreieck wird gezeigt, dass eine analytische Behandlung bei einer symmetrischen Konfiguration möglich ist. In diesem Modell hat der Hamiltonoperator einen maximal verschränkten, antisymmetrischen Eigenzustand, welcher eine Superposition von allen involvierten Atomen mit jeweils orthogonal ausgerichteten Dipolübergängen ist. Dieser Zustand besitzt maximale Subradianz, im Gegensatz zu Superradianz. Darüber hinaus entkoppelt dieser Eigenzustand vollständig vom Vakuum und zerfällt damit nichtmehr spontan in den Grundzustand aber dennoch induzieren ungleichförmige Zerfallskopplungskoeffizienten eine endliche Lebensdauer.
Numerische Simulationen mit verschiedenen Dipolorientungen und interatomaren Abständen werden dargestellt und die jeweils auf ihre subradianten Eigenschaften untersucht.

Danksagung

An dieser Stelle möchte ich mich bei all denjenigen bedanken, die mich während der Anfertigung dieser Masterarbeit unterstützt und motiviert haben.

Zuerst gebührt mein Dank Herrn Prof. Ritsch, der meine Masterarbeit betreut und begutachtet hat. Für die hilfreichen Anregungen und die konstruktive Kritik bei der Erstellung dieser Arbeit möchte ich mich herzlich bedanken.

Auch bedanken möchte ich mich bei Laurin Ostermann, David Plankensteiner und den Kolleginnen und Kollegen aus der Forschungsgruppe von Herrn Prof. Ritsch für die Hilfestellungen, Vorschläge und Diskussionen.

Meiner Freundin Marta danke ich besonders für den starken emotionalen Rückhalt über die Dauer meines gesamten Studiums in Innsbruck.

Abschließend möchte ich mich bei meinen Eltern Maria und Franz und meiner Schwester Eva bedanken, die mir mein Studium durch ihre Unterstützung ermöglicht haben.

Für Marta, Eva, Maria, Franz

Contents

Chapter 1

Introduction

One of the processes in nature that is hard to control is the spontaneous emission of photons from atoms. It can be attributed to fluctuations of the electromagnetic vacuum. As the decay process occurs randomly in time, it can be a problem for experiments that require prepared excited states, to be stable over an extended period of time, for instance in the storage of quantum information. A way to slow down the spontaneous emission rate of atoms in a cloud, an array or optical lattice is to prepare the atoms in antisymmetric superpositions in such a way, that the decay channels block each other. Such subradiant states have already been observed in experiments [1]. In the present thesis the special case of three or more V-type emitters will be investigated.

As was predicted by Robert Dicke in 1954 [2], the collective effects in a collection of identical atoms can enhance (superradiance) or suppress (subradiance) spontaneous emission. On one hand superradiance occurs if all dipoles in the system contribute constructively to the emission process. Dicke showed, that this effect is strongest for symmetric states, such that there is constructive interference between the radiation of different atoms.

On the other hand, subradiance occurs, when the dipoles are in antisymmetric superposition states, which means their total dipole moment expectation value is minimized or even sums up to zero. In this case the collective decay slows down considerably. Ultimately the dipoles could even completely decouple from the vacuum fluctuations and external electromagnetic fields and thereby stopping spontaneous emission altogether.

Superradiant states are short lived and emit an intense light pulse, which is easy to observe, but subradiant states are long lived and very susceptable to interference effects of various kinds such as Doppler shifts, Lamb shifts, atomic motion and AC-Stark shifts[3] and these problems can for instance be circumvented by using ultacold atoms with interatomic distances smaller than the atomic transition wavelength λ_0, where subradiance is present and can become dominant over longer time.

The antisymmetric states or so-called dark states that constitute the subradiant system can store photons and the quantum information that is stored

in them over long time periods. These subradiant states can therefore be used for quantum storage devices [4] and there are even protocols that propose to switch between the sub- and superradiant states, where the subradiant states are used for information storage and superradiant states are used for fast read-out of the quantum information [5]. Lastly an important application is optical atomic clocks in which the accuracy depends on the coherence time of collective atomic excitations.

In this thesis, however, we are considering the dissipative dynamics of three level V-type emitters decaying collectively and investigate the conditions under which atomic excitation energy is stored in the atomic system for as long as possible.
We are interested here in V-type systems specifically, because in principle for N atoms they can store up to N-1 excitations as we will show in chapter 2 under the condition that their transition dipoles are orthogonal and therefore independent. The case for Λ-type systems is discussed in [6] but in this case only 1 excitation can be stored in dark states per N atoms and ladder-type systems will not be considered, since their transition dipole moments are not independent. They alse deserve further investigation in furture work.

Chapter 2

Theoretical Concepts

2.1 Model description for atoms

In general a free atom has an infinite number of bound states. Often only a few are important for the dynamics in a particular experiment. Here we are dealing largly with three level quantum systems interacting with each other as part of an open quantum system coupled to the same resevoir. In particlular for three interacting 3-level emitters, the Hilbert space that is necessary for describing such a system can be written as $\mathcal{H} = (\mathbb{C}^3)^{\otimes 3}$, therefore the Hilbert space is 27 dimensional.

Important for the present analytical and numerical calculations are the non-hermitian atomic transition operators between energy levels and in particular for the three three level V-type systems there are 12 of them, which are given by

$$\hat{\sigma}_1^{i+}, \hat{\sigma}_1^{i-}, \hat{\sigma}_2^{i+}, \hat{\sigma}_2^{i-}, \quad i = 1, 2, 3 \tag{2.1}$$

In Fig.(2.1), the atomic raising operator for the first atom from the ground-state to the excited state $|e_2\rangle$ is shown:

$$\hat{\sigma}_2^{1+} = |e_2\rangle\langle g| \otimes \mathbb{1}_3 \otimes \mathbb{1}_3 = \begin{bmatrix} 0 & 0 & 0 \\ 0 & 0 & 1 \\ 0 & 0 & 0 \end{bmatrix} \otimes \mathbb{1}_3 \otimes \mathbb{1}_3 \tag{2.2}$$

where the matrix representation is based on the standard euclidean basis. With this the free atomic Hamiltonian can be written as

$$H_A = \sum_{i=1}^{3} \hbar\omega_i \hat{\sigma}_j^{i+} \hat{\sigma}_j^{i-} \tag{2.3}$$

where degenerate excited energy levels are assumed.

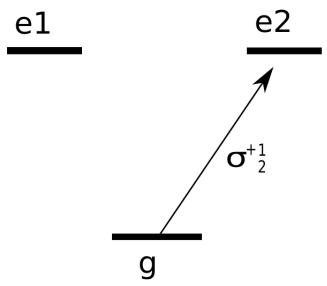

FIGURE 2.1: Schematic drawing of an individual three level V-System with the transition from the ground state to the second excited state.

2.2 Time evolution in the interaction picture

In general the total system Hamiltonian consists of the free part H_A and the interaction H_{int}. In order to determine the time evolution of the atomic density operator only due to the interaction part of the Hamiltonian, it is helpful to transform the state vectors and operators into the interaction picture with no explicit time dependence. This plays an integral part in deriving the master equation for the atomic density operator. (In the following, the hats above the operators are dropped, since the calculation involves only quantum mechanical quantities.) First the combined Hamilton-operator is split into a time independent part and an interaction part $H = H_A + H_{int}$ where H_A is the non-interacting stationary part and then new state vectors are defined by

$$|\psi_I(t)\rangle = e^{itH_A/\hbar}|\psi_S(t)\rangle = U_0^\dagger|\psi_S(t)\rangle, \tag{2.4}$$

where $|\psi_S(t)\rangle$ obeys the Schrödinger eqation

$$i\hbar\partial_t|\psi_S(t)\rangle = H|\psi_S(t)\rangle \tag{2.5}$$

In order for the expectation values to remain invariant the operators have to be transformed via $\hat{O}_I(t) = U_0^\dagger(t)\hat{O}_S U_0(t)$.

After using the definition and the Schrödinger eq. the equation of motion for the state vector in the interaction picture is given by

$$i\hbar\partial_t|\psi_I(t)\rangle = H_{int}|\psi_I(t)\rangle, \tag{2.6}$$

which upon formal integration leads to the following solution

$$|\psi_I(t)\rangle = U_I(t)|\psi_I(0)\rangle, \tag{2.7}$$

where $U_I(t) = T\ exp\Big(-\frac{i}{\hbar}\int_0^t dt' H_{int}(t')\Big)$ with the time ordered expansion of the exponential.
From this follows that $i\hbar\partial_t U_I(t) = H_{int}(t)U_I(t)$ and $U_I(0) = \mathbb{1}$.

For the density operator in the Schrödinger picture the time evolution is given by

$$i\hbar\partial_t\rho_S(t) = [H, \rho_S(t)]$$

via $i\hbar\partial_t|\psi_S(t)\rangle = H|\psi_S(t)\rangle$.
Similarly in the interaction picture it is given by

$$i\hbar\partial_I\rho_I(t) = [H_{int}, \rho_I(t)]$$

via $i\hbar\partial_t|\psi_I(t)\rangle = H_{int}|\psi_I(t)\rangle$.

Lastly the transformation back to the Schrödinger picture is done in the following manner: $O_S = U_0(t)O_I(t)U_0^\dagger(t)$.

2.3 Open Quantum Systems

In open quantum systems we include the interaction of a system of interest with the environment. Therefore the Hilbert space can be expressed as $\mathcal{H} = \mathcal{H}_S \otimes \mathcal{H}_E$ with the combined density operator $\rho = \rho_S \otimes \rho_E \in \mathcal{H}$.

The dynamics of the combined system is given by $\rho(t) = U(t)\rho(0)U(t)^\dagger = \mathcal{V}(t)\rho(0)$ and by taking the partial trace over the environment takes the form [7]

$$\rho_S(t) = Tr_E\{U(t)\rho(0)U(t)^\dagger\} \tag{2.8}$$

and by assuming that the initial state between the system and the environment is a product state of the form $\rho(0) = \rho_S(0) \otimes \rho_E(0)$. Then the right hand side of Eq. 2.8 defines a dynamical map $\mathcal{V}(t)$ acting solely on system S.

On the other hand we have seen that the von Neumann equation for a general density operator is given by

$$\partial_t\rho = -\frac{i}{\hbar}[H, \rho]. \tag{2.9}$$

Now we can define the superoperator $\mathcal{L}$ via $\mathcal{L}[\rho_S] = -i/\hbar[H, \rho_S]$, that means it acts on operators and returns operators. [8]

Therefore the equation of motion can formally be written as

$$\partial_t \rho_S(t) = \mathcal{L}[\rho_S(t)], \tag{2.10}$$

where the superoperator can be quit complex containing decay rates describing incoherent dissipation processes in the system. These decay processes lead to a stationary state of the system of the form $\partial_t \rho_S = 0$, which is normally the ground state ρ_G of the system containing no excitation, since all of them will dissipate their energy into the environment. But still their exist states, although not purely stationary under $\mathcal{L}$, that decay very slowly due to their antisymmetry in the dipole moment orientations.

In summary, an open quantum system is described as a subsystem of a combined system S + E, S being the Subsystem and E the environment. For the equation of motion or master equation we consider only the dynamics of the reduced system $\rho_S(t) = Tr_f(\rho(t))$, with the Hamiltonian of the combined system is given by $H = H_S + H_f + H_{int}$ and where H_S describes the atomic system, H_f the field of radiation and H_{int} the interaction between system and field.
By transforming into the interaction picture $H'_{int}(t) = e^{iH_0 t} H_{int} e^{-iH_0 t}$, and assuming that $H_0 = H_S + H_f$ is a closed system we use the von Neumann euqation for the density operator to derive a equation of motion with the following assumptions along the way:

- At $t = 0$ we assume no correlations between the system S and the field E. Therefore the initial density operator is factorized into $\rho(0) = \rho_S(0) \otimes \rho_f(0)$.
- The Born approximation, meaning the density operator factorises at all times as $\rho(t) \approx \rho_S(t) \otimes \rho_f(0)$. This relies on the interaction via H_{int} to be weak and that the environment is a large system, being in constant thermal equillibrium and thus any dissipation coming from the enclosed subsytem gets thermalized very fast in comparison to the atomic system's relaxation time. (Markov approximation) [7]
- $\rho_S(t)$ to be local in time, which means as a consequence of the Markov approximation we can write $\rho_S(t+\tau) = \rho_S(t) + \rho_S(\tau)$ for $t, \tau > 0$, where ρ_S depends now only on the present state and not on memory effects from previous times.

2.4 Selection rules and angular momentum conservation

In V-type systems with degenerate magnetic sublevels as excited states, meaning with the same angular momentum quantum number j, the dipole matrix vectors are complex and in particular for radialsymmetric potentials the angular momentum is conserved and the z-component of the angular mommentum operator obeys the following relations [9]:

$$[\hat{L}_z, \hat{z}] = 0, \quad [\hat{L}_z, \hat{x} \pm i\hat{y}] = \pm(\hat{x} \pm i\hat{y}). \tag{2.11}$$

If we take the matrix elements where the eigenstates are labled with their quantum numbers n,l,m, we have

$$\begin{aligned} (m' - m)\langle n', l', m'|\hat{z}|n, l, m\rangle &= 0, \\ (m' - m \mp 1)\langle n', l', m'|\hat{x} \pm i\hat{y}|n, l, m\rangle &= 0. \end{aligned} \tag{2.12}$$

where $\hat{L}_z|m\rangle = m|m\rangle$.

This implies that the matrix elements of $\hat{z}$ are only non-vanishing for $m' = m$, whereas the matrix elements of $\hat{x} \pm i\hat{y}$ vanish only for $m' = m \pm 1$.
If the magnetic quantum number m changes by one unit than the z-component vanishes and the dipole moment rotates in the x-y plane, while emitting circular polarized light in the z direction. [9]

Similarly using $\left[\hat{L}^2, \left[\hat{L}^2, \hat{x}\right]\right] = 2\hbar^2\left\{\hat{x}, \hat{L}^2\right\}$ and $\hat{L}^2|l, m\rangle = \hbar^2 l(l+1)|l, m\rangle$ and taking the matrix elements of the first equation, the selection rule $l' = l+1$ can be deduced. Here $\{A, B\}$ is the anticommutator of the two operators A and B.

Therefore the so called selection rules for dipole radiation show how a V-type system with two independent transitions as shown in Fig.(2.2) can be described.

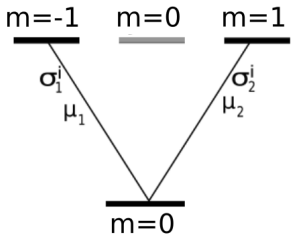

FIGURE 2.2: V-System with the upper levels $l = 1$ and the lower level $l = 0$

As another consequence, only transitions from different atoms between $m = -1$ and $m = 0$ can directly interact amongst each other, as well as transitions between $m = +1$ and $m = 0$, since in each case the light has a particular polarization and the transition are only receptible to those particular polarizations. Although the transition cannot interact directly, they can still interact via the electromagnetic vacuum field as will be shown below.

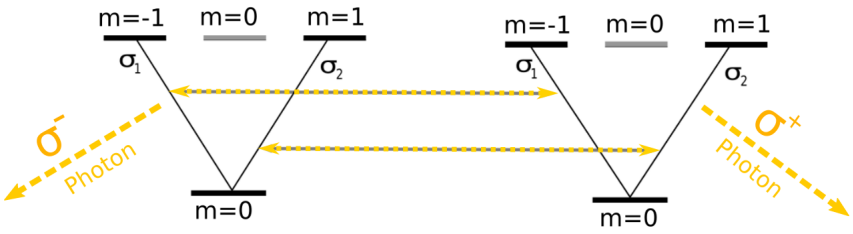

FIGURE 2.3: Transitions inside each atom are orthogonal and only interact directly with those same transitions in other identical atoms.

In Fig.(2.3) it is seen that only $\hat{\sigma}_j^i$ and $\hat{\sigma}_j^k$ for $i \neq k$ are directly coupled, therefore $\sigma_1 \perp \sigma_2$

The selection rules become clear, when considering the radiation of electromagnetic waves, where photons of angular momentum one are emitted. After the emission the angular momentum number of the electron has to change by one unit and the m quantum number by zero or ± 1, which corresponds to linear polarized or left/right circular polarized light. This process is illustrated in Fig.(2.3).

2.5 Dynamics of atomic excitations

We consider a collection of N identical atoms separated by a small distance, which are coupled to the quantized electromagnetic field. Each atom is described as a V-type system with N-1 nearly degenerate excited states and a single ground state. Therefore we have the closely lying excited energy levels: $\omega_1 \neq \omega_2 \neq ... \neq \omega_{N-1}$
With this the combined Hamiltonian of the System interacting with its electromagnetic environment reads

$$\hat{H} = \hat{H}_a + \hat{H}_f + \hat{H}_{int} \tag{2.13}$$

where

$$\hat{H}_a = \sum_{i=1}^{N} \sum_{j=1}^{N-1} \hbar\omega_j \hat{\sigma}_j^{i+} \hat{\sigma}_j^{i-} \tag{2.14}$$

$$\hat{H}_f = \sum_{\vec{k},\lambda} \hbar\omega_k \hat{a}^\dagger_{\vec{k},\lambda} \hat{a}_{\vec{k},\lambda}, \tag{2.15}$$

with $\hbar = 1$ and the atomic transition operators are given by

$$\hat{\sigma}_j^{i+} = |e_j^i\rangle\langle g_i| \qquad\qquad \hat{\sigma}_j^{i-} = |g_i\rangle\langle e_j^i|, \tag{2.16}$$

where e_j^i is the jth excited energy level in the ith atom and g_i its ground state.

All dipole transitions in atom i are assumed to be at the same spatial location $\vec{r_i}$ and the atoms are assumed to be fixed at their positions.

$$\hat{H}_{int} = -\sum_{i=1}^{N} \sum_{j=1}^{N-1} \hat{\vec{d}}_j^i \cdot \hat{\vec{E}}(\vec{r_i}). \tag{2.17}$$

The electric field operator $\vec{E}(\vec{r_i}, t)$ in quantized form is given by [23]

$$\hat{\vec{E}}(\vec{r_i}, t) = i \sum_{\vec{k},\lambda} \left(\frac{2\pi\hbar\omega_k}{V} \right)^{1/2} \vec{e}_{\vec{k},\lambda} [\hat{a}_{\vec{k},\lambda}(t) e^{i\vec{k}\cdot\vec{r_i}} + H.c.] \tag{2.18}$$

Here $\hat{a}_{\vec{k},\lambda}, \hat{a}^\dagger_{\vec{k},\lambda}$ represent the bosonic ladder operators of a field mode with propagation vector $\vec{k}$ and polarization λ, whereas $\omega_k = kc$ ($|\vec{k}| = k$) represents the angular frequency of the k-mode and the corresponding unit polarization vector is denoted by $\vec{e}_{\vec{k},\lambda}$.

The dipole matrix elements are written as

$$\hat{\vec{d}}_j^i = \vec{\mu}_j^i |e_j^i\rangle\langle g_i| = \vec{\mu}_j^i \hat{\sigma}_j^{i+}. \tag{2.19}$$

We assume that the different transition dipole matrix elements in atom i are orthogonal, therefore

$$\vec{d}_j^i \cdot \vec{d}_{j'}^{i*} = 0, \tag{2.20}$$

where we have taken the complex conjugate, since the matrix elements can be complex in general.

By transforming into the interaction picture via the transformation

$$\hat{O}_{int}(t) = U(t)\hat{O}_{int}U^\dagger(t) \tag{2.21}$$

with the unitary operator $U(t) = e^{i/\hbar(H_a+H_f)t}$, the interaction Hamiltonian becomes

$$\hat{H}_{int}(t) = -\sum_{i=1}^{N}\sum_{j=1}^{N-1}\sum_{\vec{k},\lambda} i\left(\frac{2\pi\hbar\omega_k}{V}\right)^{1/2}\left(\vec{\mu}_j^i\hat{\sigma}_j^{i+}e^{i\omega_j t}\cdot\left(\vec{e}_{\vec{k},\lambda}a_{\vec{k},\lambda}e^{i(\vec{k}\cdot\vec{r}_i-\omega_k t)}+H.c.\right)+H.c.\right) \tag{2.22}$$

Now to derive the equation of motion for the atomic part of the system we start with the density matrix of the combined atom-field system $\hat{\rho}(t)$, which satisfies the Liouville equation of motion

$$\frac{\partial\hat{\rho}}{\partial t} = -i/\hbar[\hat{H}_{int}(t),\hat{\rho}]. \tag{2.23}$$

Formal integration of Eq. (2.23) leads to

$$\rho(t) = \rho(0) - i/\hbar\int_0^t ds\ [H_{int}(s),\rho(s)], \tag{2.24}$$

and by inserting this result back into Eq. (2.23) we arrive at

$$\frac{\partial\hat{\rho}_a}{\partial t} = -1/\hbar^2\int_0^t ds\ Tr_f\{[\hat{H}_{int}(t),[\hat{H}_{int}(s),\hat{\rho}(s)]]\} - 1/\hbar\underbrace{i\ Tr_f\{[\hat{H}_{int}(t),\hat{\rho}(0)]\}}_{=0}, \tag{2.25}$$

where the second term vanishes because we assume initially no interaction between the atoms and the field ($\hat{\rho}(0) = \hat{\rho}_a(0)\otimes\hat{\rho}_f(0)$) and therefore no first-order correlations.

Furthermore we make the Born-Approximation, which in our case means weak interaction between the atomic system and the field at later times and therefore the field is approximately constant in time in the time frame of the atomic dynamics:

$$\hat{\rho}_f(t) \approx \hat{\rho}_f \Rightarrow \hat{\rho}(t) \approx \hat{\rho}_a(t) \otimes \hat{\rho}_f. \tag{2.26}$$

With this, Eq. (2.25) takes on the following form

$$\frac{\partial \hat{\rho}_a}{\partial t} = -1/\hbar^2 \int_0^t ds\, Tr_f\{[\hat{H}_{int}(t), [\hat{H}_{int}(s), \hat{\rho}_a(t) \otimes \hat{\rho}_f]]\}, \tag{2.27}$$

where under the weak interaction assumption we have replaced $\hat{\rho}_a(s)$ by $\hat{\rho}_a(t)$.

Next we make the substitution $s \to t - s$ ($ds = dt$) and under the Markov-Approximation [10], which states that memory effects over which correlations in the field decay, are very short-lived and therefore the integrand vanishes quickly for $t < t - s$, we extend the integration limit to infinity.

Also since the relaxation time of the quantum optical system due to the interaction with the field usually lie in the range of 10^{-6}[s], but the timescale over which correlations in the field decay are given by the inverse of the atomic transition frequency and lie in the range of 10^{-14}[s], we see that the correlations vanish rapidly compared to the timescale of the Master equation of the atomic sytem.

From this we obtain a Markovian Master equation for the atomic system

$$\frac{\partial \hat{\rho}_a}{\partial t} = -1/\hbar^2 \int_0^\infty ds\, Tr_f\{[\hat{H}_{int}(t), [\hat{H}_{int}(t-s), \hat{\rho}_a(t) \otimes \hat{\rho}_f]]\}. \tag{2.28}$$

The trace over the bosonic field operators inside the integral in Eq. (2.28) corresponds to their vacuum expectation values and are given by [6]

$$\begin{aligned} Tr_f\{\hat{\rho}_f a^\dagger_{k,\lambda} a_{k',\lambda'}\} = 0, \quad Tr_f\{\hat{\rho}_f a_{k,\lambda} a^\dagger_{k',\lambda'}\} = \delta_{kk'}\delta_{\lambda\lambda'}(1 + N(\omega_{k'})) \\ Tr_f\{\hat{\rho}_f a_{k,\lambda} a_{k',\lambda'}\} = 0, \quad Tr_f\{\rho_f a^\dagger_{k,\lambda} a^\dagger_{k',\lambda'}\} = \delta_{kk'}\delta_{\lambda\lambda'} N(\omega_{k'}). \end{aligned} \tag{2.29}$$

In the case when the environment is in thermal equillibrium, and therefore the environment density operator can be expressed as [13]

$$\hat{\rho}_f = \frac{e^{-H_f/k_BT}}{tr\{e^{-H_f/k_BT}\}}, \tag{2.30}$$

where k_B is the Boltzmann constant, and T is the environment temperature. Then the Bose-Einstein occupation number is given by $N(\omega_k) = (e^{\omega_k/k_BT})^{-1}$, and in the case of $T \to 0$ we see that $N(\omega_k) \approx 0$. [11]

We can neglect terms of the form $\hat{\sigma}_j^{i+}\hat{\sigma}_j^{i+}$ and $\hat{\sigma}_j^{i-}\hat{\sigma}_j^{i-}$ since applying them to the atomic density operator just gives 0.

In calculating the time integral, integrands of the following form have to be resolved

$$\int_0^\infty e^{it'\omega}\, dt' = \lim_{\epsilon\to 0}\lim_{t\to\infty}\int_0^t e^{it'\omega-\epsilon t'}dt' = \lim_{\epsilon\to 0}\lim_{t\to\infty}\frac{1}{i\omega-\epsilon}\Big(e^{it\omega-\epsilon t}-1\Big) \tag{2.31}$$

and by taking the limit $t \to \infty$ and by either using the Dirac-Identity or taking the appropriate complex contour we arrive at the following functional

$$\lim_{\epsilon\to 0}\frac{i}{\omega+i\epsilon} = iP\Big(\frac{1}{\omega}\Big) + \pi\delta(\omega), \tag{2.32}$$

where P denotes the principal value of the integral and $\delta(\omega)$ is the Dirac delta function.

We assume, that the excited energy levels are nearly degenerate and approximate $\omega_j \approx \omega_{j'} = \omega_0$, which is valid when considering real atomic systems like Strontium for instance, to arrive at the following master equation of motion for the atomic density operator after doing the algebra

$$\begin{aligned}\frac{\partial\hat{\rho}_a}{\partial t} = &-\sum_{i,k}^{N}\sum_{j,j'}^{N-1}\Gamma_{jj'}^{ik}\Big(\hat{\sigma}_j^{i+}\hat{\sigma}_{j'}^{k-}\hat{\rho}_a - 2\hat{\sigma}_j^{k-}\hat{\rho}_a\hat{\sigma}_{j'}^{i+} + \hat{\rho}_a\hat{\sigma}_j^{i+}\hat{\sigma}_{j'}^{k-}\Big)\\ &+\sum_{i\neq k}^{N}\sum_{j,j'}^{N-1} i\,\Omega_{jj'}^{ik}[\hat{\sigma}_j^{i+}\hat{\sigma}_{j'}^{k-},\hat{\rho}_a],\end{aligned} \tag{2.33}$$

where we have introduced the dissipative and coherent coupling coefficients

$$\Gamma_{jj}^{ii} = \gamma_j = \sum_{k,\lambda} \left(\frac{2\pi\omega_k}{\hbar V} \right) \pi\delta(\omega_0 - \omega_k) |\vec{\mu_j^i} \cdot \vec{\epsilon}_{k,\lambda}|^2 \tag{2.34}$$

$$\Gamma_{jj'}^{ik} = \sum_{k,\lambda} \left(\frac{2\pi\omega_k}{\hbar V} \right) \pi\delta(\omega_0 - \omega_k) (\vec{\mu_j^i} \cdot \vec{\epsilon}_{k,\lambda})(\vec{\mu_{j'}^k} \cdot \vec{\epsilon}_{k,\lambda}) e^{i\vec{k}\cdot(\vec{r}_i - \vec{r}_k)} \tag{2.35}$$

$$\Omega_{jj'}^{ik} = \sum_{k,\lambda} \left(\frac{2\pi\omega_k}{\hbar V} \right) \left(\frac{1}{\omega_0 - \omega_k} + \frac{1}{\omega_0 + \omega_k} \right) (\vec{\mu_j^i} \cdot \vec{\epsilon}_{k,\lambda})(\vec{\mu_{j'}^k} \cdot \vec{\epsilon}_{k,\lambda}) e^{i\vec{k}\cdot(\vec{r}_i - \vec{r}_k)} \tag{2.36}$$

In Fig. (2.4) the collective couplings between two atoms are shown.

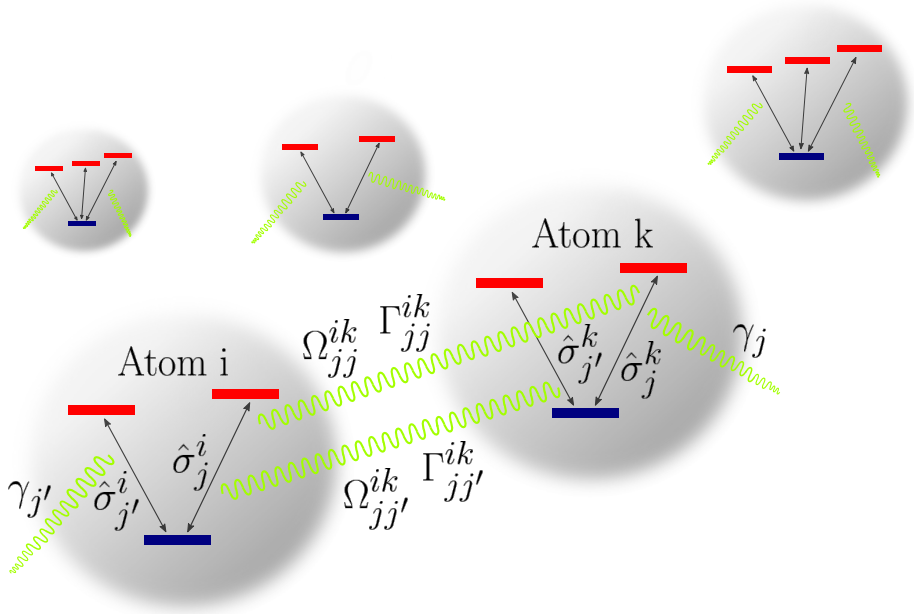

FIGURE 2.4: Illustration of the atomic system with an arbitrary arrangement, where the dissipative coupling terms between two atoms are shown.

Now we go over to a continous vacuum mode spectrum i.e. $\sum_{\vec{k},\lambda} \rightarrow V/(2\pi)^3 \int d^3k \sum_\lambda$, and look closely at the sum over the mode functions, where $\vec{k} \perp e_{\vec{k},1} \perp e_{\vec{k},2}$ and $e_{\vec{k},2}$ points out of the page and μ_i along the z-Axis as shown in Fig.(2.5)

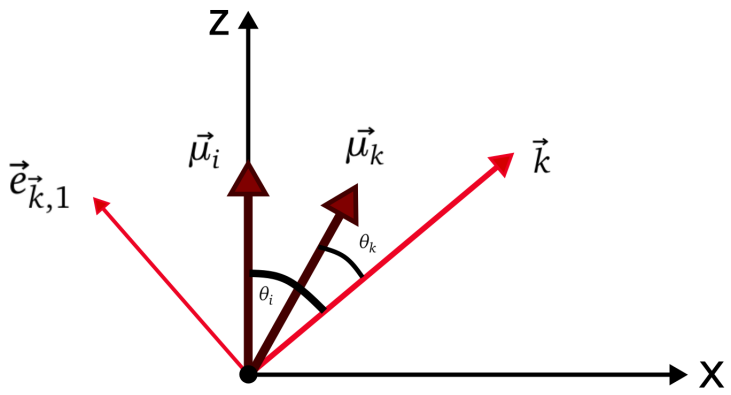

FIGURE 2.5: Orientation of dipoles and polarization vectors, where $e_{\vec{k},2}$ points out of the page. Here $\vec{\mu_i}$ and $\vec{\mu_k}$ are two transition dipole vectors either belonging to the same atom or different atoms and different transitions.(For two transitions of the same atom, the transition dipole vectors would be orthogonal to each other.)

From Figure 2.5 we deduce the resolution of the summation over the polarization components:

$$\sum_{\lambda}(\vec{\mu_i}\cdot\vec{\epsilon}_{k,\lambda})(\vec{\mu_k}\cdot\vec{\epsilon}_{k,\lambda}) = \mu^2(e_{\mu_i}\cdot e_{k,1})(e_{\mu_k}\cdot e_{k,1}) = \mu^2 sin(\theta_i)sin(\theta_k)$$
$$= \mu^2 cos(\theta_i-\theta_k) - \mu^2 cos(\theta_i)cos(\theta_k) = \mu^2\Big[e_{\mu_i}\cdot e_{\mu_k} - (e_{\mu_i}\cdot e_{\vec{k}})(e_{\mu_k}\cdot e_{\vec{k}})\Big] \tag{2.37}$$

where $|\vec{\mu_i}| = |\vec{\mu_k}| =: \mu$, $e_{\vec{\mu}} = \vec{\mu}/\mu$ and $e_{\vec{k}} = \vec{k}/k$.

Now the coupling terms in Eq.(2.34–2.36) become [6]

$$\gamma_j = \frac{2\mu_j^2}{3\hbar}\left(\frac{\omega_0}{c}\right)^3 \tag{2.38}$$

$$\Gamma^{ik}_{jj'} = \frac{1}{\hbar}\left(\vec{\mu^i_j}\cdot Im\{\chi\}\cdot\vec{\mu^{k*}_{j'}}\right), \quad \Omega^{ik}_{jj'} = \frac{1}{\hbar}\left(\vec{\mu^i_j}\cdot Re\{\chi\}\cdot\vec{\mu^{k*}_{j'}}\right),$$

where $\vec{d^i_j}\cdot Im\{\chi\}\cdot\vec{d^{k*}_{j'}} = \mu_j\ \mu_{j'}\ Im\{\chi^{ik}_{jj'}(\omega_0)\}$ is the imaginary part of the tensor component $\chi^{ik}_{jj'}(\omega_0)$ which is given by

$$\chi^{ik}_{jj'}(\omega_0) = \left[\hat{\mu}^i_j \cdot \hat{\mu}^k_{j'}\left(\frac{k_0^2}{r_{ik}} + \frac{ik_0}{r_{ik}^2} - \frac{1}{r_{ik}^3}\right) - (\hat{\mu}^i_j \cdot \hat{r}_{ik})(\hat{\mu}^k_{j'} \cdot \hat{r}_{ik})\left(\frac{k_0^2}{r_{ik}} + \frac{3ik_0}{r_{ik}^2} - \frac{3}{r_{ik}^3}\right)\right] e^{ik_0 r_{ik}}. \tag{2.39}$$

Here $k_0 = \frac{\omega_0}{c}$, $r_{ik} = |\vec{r}_i - \vec{r}_k|$, $\hat{r}_{ik} = \vec{r}_{ik}/r_{ik}$ and $\hat{\mu}^i_j = \vec{\mu}^i_j/\mu_j$.

It should be noted, that $2\gamma_j$ corresponds to the single atom spontaneous emission rate from the state $|e_j\rangle$ to the ground state $|g\rangle$. The dipole-dipole interaction on the other hand is completely determined by the tensor χ.
The tensor component $\chi^{ik}_{jj'}$ is a geometric quantity and relates the transiton dipole unit vector $\vec{\mu}_j$ in atom i with $\vec{\mu}_{j'}$ of atom k.
The crucial steps for deriving $\chi^{ik}_{jj'}$ are presented in the Appendix [7].

It is interesting to note, that although the transition dipoles $\vec{\mu}^i_j$ and $\vec{\mu}^k_{j'}$ might be othogonal, $(\vec{\mu}^i_j \cdot \vec{r}_{ik})$ and $(\vec{\mu}^k_{j'} \cdot \vec{r}_{ik})$ might not be orthogonal, and lead to a non-zero contribution in the dipole-dipole coupling. This contributions manifest themselves in the so called dipole-dipole cross coupling coefficients $\Gamma^{ik}_{jj'}$ and $\Omega^{ik}_{jj'}$ for $i \neq k$, $j \neq j'$ and couple pairs of orthogonal dipoles.

With the help of the following functions

$$P_r(r) = \frac{\cos r}{r} - \frac{\sin r}{r^2} - \frac{\cos r}{r^3}, P_i(r) = \frac{\sin r}{r} + \frac{\cos r}{r^2} - \frac{\sin r}{r^3}$$

$$Q_r(r) = \frac{\cos r}{r} - 3\frac{\sin r}{r^2} - 3\frac{\cos r}{r^3}, Q_i(r) = \frac{\sin r}{r} + 3\frac{\cos r}{r^2} - 3\frac{\sin r}{r^3}; \quad r = k_0 r_{ik},$$

we can rewrite the radiative coupling terms for real dipole matrix elements as follows

$$\Gamma^{ik}_{jj'} = \mu_j \mu_{j'} Im\{\chi^{ik}_{jj'}(\omega_0)\} = \frac{3\gamma}{4}\Big(\hat{\mu}^i_j \cdot \hat{\mu}^k_{j'} P_i(r_{ik}) - (\hat{\mu}^i_j \cdot \hat{r}_{ik})(\hat{\mu}^k_{j'} \cdot \hat{r}_{ik}) Q_i(r_{ik})\Big)$$

$$\Omega^{ik}_{jj'} = \mu_j \mu_{j'} Re\{\chi^{ik}_{jj'}(\omega_0)\} = \frac{3\gamma}{4}\Big(\hat{\mu}^i_j \cdot \hat{\mu}^k_{j'} P_r(r_{ik}) - (\hat{\mu}^i_j \cdot \hat{r}_{ik})(\hat{\mu}^k_{j'} \cdot \hat{r}_{ik}) Q_r(r_{ik})\Big)$$

and $\gamma = 2\gamma_j$ is the spontaneous emission rate of a single transition given by $\frac{4|\vec{d}_j|^2}{3\hbar}(\frac{\omega_0}{c})^3$.

For a quick illustration of the coupling coefficient, let us consider three V-type atoms in an equilateral triangle configuration, an example which will be investigated later in much more detail. The scheme is shown in Fig.(3.1), where the dipole orientations are such that $\Gamma^{ik}_{jj'} = \delta_{jj'}\Gamma_j$ and $\Omega^{ik}_{jj'} = \delta_{jj'}\Omega j$ reduce to two coefficients respectively.

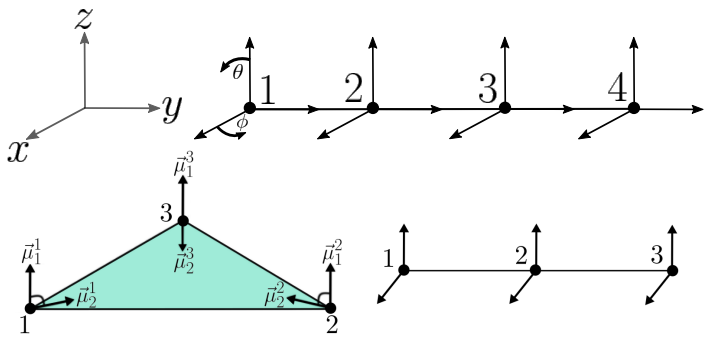

FIGURE 2.6: Equilateral triangle configuration on the lower left, where the transition dipole vectors of the second transition in each atom point towards the center of the equilateral triangle. Also shown are linear chains for three and four atoms.

The behaviour of the dipole-dipole coupling terms between two atoms is shown in Fig.(2.7)

If we go back to Eq.(2.33) and put down the equation motion for the atomic density operator in the Schrödinger picture, we arrive at

$$\partial_t \hat{\rho}_a = i[\hat{\rho}, \hat{H}] + \mathcal{L}[\hat{\rho}_a] \tag{2.40}$$

where the Hamiltonian is given by

$$\hat{H} = \sum_{j=1}^{N-1} \sum_{i}^{N} \omega_j \hat{\sigma}_j^{i+} \hat{\sigma}_j^{i-} + \sum_{i \neq k}^{N} \sum_{j,j'}^{N-1} \Omega_{jj'}^{ik} \hat{\sigma}_j^{i+} \hat{\sigma}_{j'}^{k-} \tag{2.41}$$

and describes the coherent energy-conserving part of the time evolution, and the Liouvillian super-operator,

$$\mathcal{L}[\hat{\rho}] = \sum_{i,k}^{N} \sum_{j,j'}^{N-1} \Gamma_{jj'}^{ik} \left(2\hat{\sigma}_j^{i-} \rho \hat{\sigma}_{j'}^{k+} - \hat{\sigma}_{j'}^{i+} \hat{\sigma}_j^{k-} \hat{\rho} - \hat{\rho} \hat{\sigma}_{j'}^{i+} \hat{\sigma}_j^{k-} \right) \tag{2.42}$$

stands for the dissipation of the atomic system into the surrounding electromagnetic field. The term $2\hat{\sigma}_j^{i-} \hat{\rho} \hat{\sigma}_{j'}^{k+}$ is called recycling term, which ensures that the overall population stays constant, by transfering the population decaying from the higher energy states into the lower lying energy states, while the last two terms account for the decay in the higher energy states.
In other words, our Liouvillian-Superoperator is a trace preserving map and also completely-positive, since the coefficient matrix $\Gamma_{jj'}^{ik}$ is symmetric in the

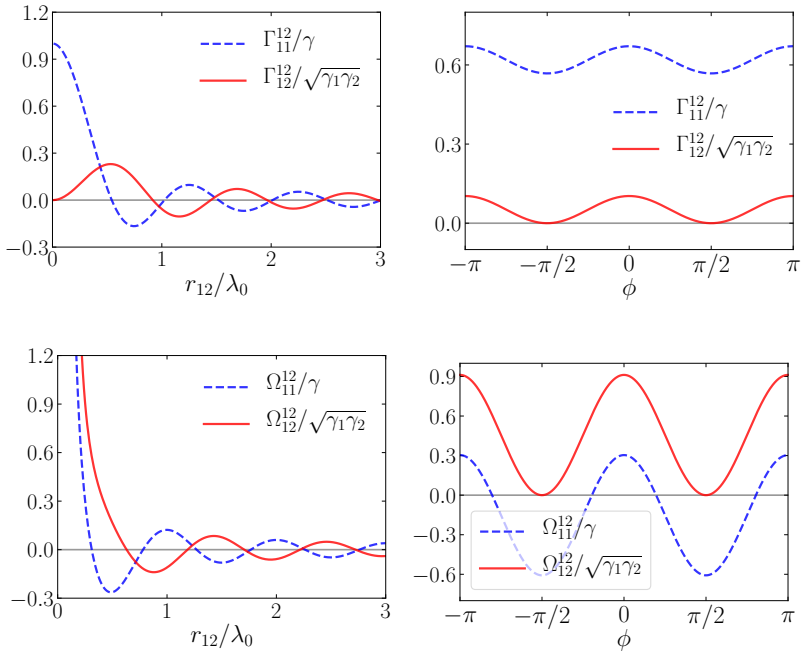

FIGURE 2.7: *Left: Plots for the dipole-dipole coupling coefficients as a function of the interatomic distance with* $\theta_1 = \pi/4$, $\theta_2 = 3\pi/4$ *for the two transitions and* $\phi = 0$. *Right: Variation of the azimuthal angle at interatomic distance* $\lambda_0/4$.

linear geometries under consideration and can therefore be diagonalized with positive-definite eigenvalues.

$$Tr(\hat{\rho}_a) = 1 \Rightarrow Tr(\mathcal{L}[\hat{\rho}_a]) = 0 \quad \text{and} \quad \mathcal{L}[\hat{\rho}_a] \geq 0 \quad . \tag{2.43}$$

Furthermore to derive eq.(2.40) we neglected all single-atom dipole shifts Ω^{ii}_{jj}, since we are only interested in the collective behaviour. Furthermore it would lead to divergences as the interatomic distance approaches zero, where this model of interatomic interaction is not valid anymore.

Geometric Parameters

The coupling matrices (Γ, Ω) in (2.34-2.36) are responsible for the collective dissipation and collective energy level shifts. They determine the collective properties of our model of N identical interacting atoms. Identical means the atomic energy levels are identical [12,13], although their individual transition dipole orientation can be different.

Both Parameters $\Gamma^{ik}_{jj'}$ and $\Omega^{ik}_{jj'}$ strongly depend an the interatomic distance r_{ik} and the orientation of the transition dipole vectors as is seen in Fig.(2.8).

In detail we can see that the interactions between $0.5 \leq \xi \leq 2$ are considerably larger when the dipoles are orthogonal to the the interatomic distance vector and parallel to each other as is the case for $\Omega^{ik}_{11} \equiv \Omega_1$ and $\Gamma^{ik}_{11} \equiv \Gamma_1$ in the equilateral triangle.

For the distance dependence, if the dipoles are parallel to each other and orthgonal to the interatomic distance vector, we get:

$$\Gamma_1(\xi) \to \begin{cases} 1, & \xi \to 0 \quad (2.44) \\ 0, & \xi \to \infty \quad (2.45) \end{cases}$$

$$\Omega_1(\xi) \to \begin{cases} -\infty, & \xi \to 0 \quad (2.46) \\ 0, & \xi \to \infty \quad (2.47) \end{cases}$$

For $\xi \to 0$ the diverging Ω_1 is neglected and $\Gamma_1 \to 1$ leads to $\Gamma^{ik}_{jj'} = \Gamma$, which means the collective decay rates all beome identical. In the other limit of $\xi \to \infty$, both functions become zero the atoms become independent emitters, infinitely far apart with decay rates $\Gamma^{ik}_{jj'} = \delta_{ik}\Gamma$.

In the case of Ω_2 and Γ_2, when the dipoles are not parallel, the dissipative coupling approaches one half, as the interatomic distance becomes zero.

The dependence on the angle θ between the transition dipoles and the interatomic distance vector is illustrated in Fig.(2.8).

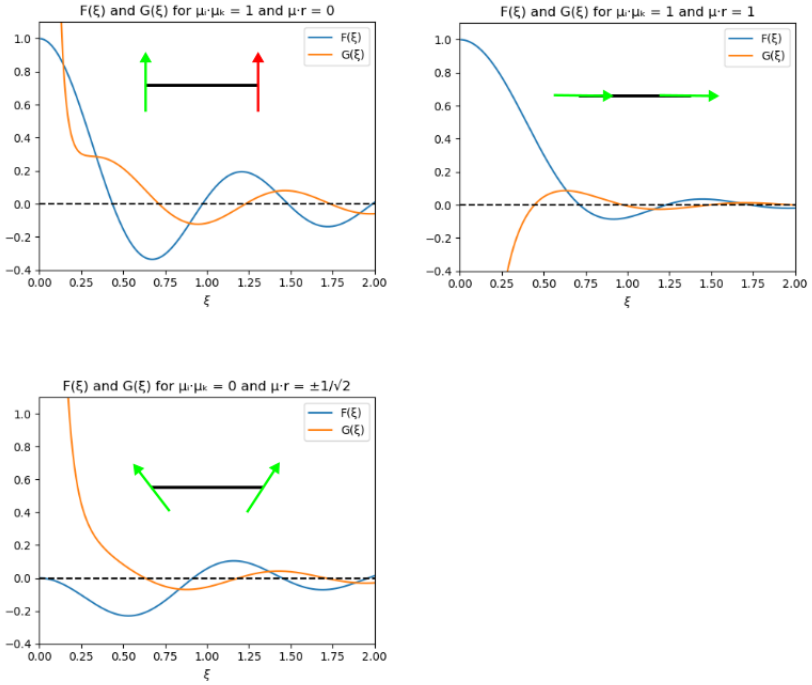

FIGURE 2.8: Angular dependence of the coupling for two parallel transition dipole vectors and mutually orthgonal ones, having an $\pi/4$ angle with the interatomic distance vector. Here $\xi = k_0 r$ and $F(\xi)$,$G(\xi)$ are plotted in units of $\sqrt{\gamma_j \gamma_{j'}}$

2.6 Dark States

It is well known that two nearby atoms exhibit a modified decay behaviour. In the simple case of two 2-level quantum emitters with states $|g\rangle$ and $|e\rangle$ the maximal superradiant and subradiant states are given in Eq.(2.48) and Fig.(2.9) (B) with a plus and a minus sign respectively.

$$|\Psi_{\pm}\rangle = \frac{1}{\sqrt{2}}(|eg\rangle \pm |ge\rangle) \tag{2.48}$$

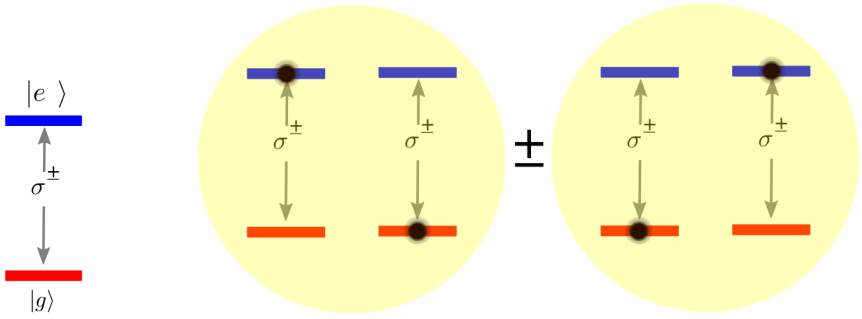

(A) (B)

FIGURE 2.9: In (A) the 2-Level-Scheme is shown and in (B) the $|\Psi_{\pm}\rangle$ states as superpositions of two 2-Level atoms.

The superradiant and the dark state of 2 particles are maximally entangled [14,15], which in this case are two of the Bell states. Similar properties hold for $N > 2$ particles with several decay channels as is shown in [6] and discussed in more detail below.

Let us list the important properties or conditions of these dark states [6,15]:

(i) They are maximally entangled (see [15])

(ii) Zero total dipole moment: $\mu_j = \langle \sum_i \hat{\sigma}_j^i \rangle_{|\Psi_d^N\rangle} = 0$

(iii) For N atoms, they need N-1 independent transitions.

(iv) Every dark state has a superradiant analogue $|\Psi_{sr}^N\rangle$ where all signs are positive.

$|\Psi_d^N\rangle$ is the generalization to N emitters and is given as follows:

$$|\Psi_d^N\rangle = \frac{1}{\sqrt{N!}} \sum_{\pi \in S_N} \mathrm{sgn}(\pi) \bigotimes_i |s_{\pi(i)}\rangle, \tag{2.49}$$

where for a system with N-1 upper states $|i\rangle = |s_i\rangle = |e_i\rangle$ and one lower lying state $|0\rangle = |s_0\rangle = |g\rangle$, as in the case for a V-System as shown in Fig.(2.10). The sum in Eq.(2.49) runs over all permutations π of N elements and $\mathrm{sgn}(\pi)$ gives a factor of $(+1)$ for cyclic permutations and (-1) otherwise, e.g. $\mathrm{sgn}(\pi(123)) = 1$ or $\mathrm{sgn}(\pi(213)) = -1$

To illustrate for the three level Λ-System with one upper state and 2 lower states we have:

$$|\Psi^3_d\rangle_\Lambda = \frac{1}{\sqrt{3!}}\Big(|eg_1g_2\rangle + |g_1g_2e\rangle + |g_2eg_1\rangle \\ -|eg_2g_1\rangle - |g_2g_1e\rangle - |g_1eg_2\rangle\Big), \tag{2.50}$$

and for the V-System with two upper states and one lower state:

$$|\Psi^3_d\rangle_V = \frac{1}{\sqrt{3!}}\Big(|ge_1e_2\rangle + |e_1e_2g\rangle + |e_2ge_1\rangle \\ -|ge_2e_1\rangle - |e_2e_1g\rangle - |e_1ge_2\rangle\Big) \tag{2.51}$$

where in comparison to the Λ-System we just make the following interchange: $e \leftrightarrow g$, $g_1 \leftrightarrow e_1$, $g_2 \leftrightarrow e_2$.

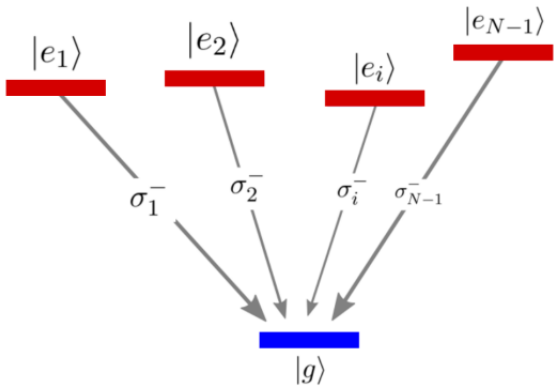

FIGURE 2.10: Multi-Level scheme of an atom with non-degenerate energy levels and dipole transitions of different spatial orientation.

Property (ii) is a consequence of the anti-symmetry of the dark state as is easily seen for $|\Psi_d^2\rangle$:

$$\mu = \langle\sigma\rangle_{|\Psi_d^2\rangle} = 0. \tag{2.52}$$

Another way to represent $|\Psi_d^3\rangle$ is via the determinant of a 3 by 3 square matrix with tensor instead of scalar multiplication and a Laplace-Expansion along the first row:

$$\begin{vmatrix} |e_1\rangle & |e_2\rangle & |g\rangle \\ |e_1\rangle & |e_2\rangle & |g\rangle \\ |e_1\rangle & |e_2\rangle & |g\rangle \end{vmatrix} = \tag{2.53}$$

$$\begin{aligned} &= |e_1\rangle \otimes \big(|e_2\rangle \otimes |g\rangle - |g\rangle \otimes |e_2\rangle\big) \\ &\quad -|e_2\rangle \otimes \big(|e_1\rangle \otimes |g\rangle - |g\rangle \otimes |e_1\rangle\big) \\ &\quad +|g\rangle \otimes \big(|e_1\rangle \otimes |e_2\rangle - |e_2\rangle \otimes |e_1\rangle\big) \\ &\propto |\Psi_d^3\rangle, \end{aligned} \tag{2.54}$$

here the subdeterminants are also entangled states in their respectively reduced Hilbert space and product states such as $|g\rangle\otimes\big(|e_1\rangle\otimes|e_2\rangle - |e_2\rangle\otimes|e_1\rangle\big) = |g\rangle(|e_1e_2\rangle - |e_2e_1\rangle)$ show subradiance, as will be shown in numerical simulations below and was demonstrated for the three level Λ-System in [6] and [16].

Chapter 3

Analytical treatment of collective dynamics in a V-type System

3.1 Symmetrical Configuration

In general it is not possible to obtain analytical expressions for the eigenstates and lifetimes of the dipole coupled Hamiltonian especially for larger system sizes and more energy levels per atom. Furthermore the dimension of the physical Hilbert space grows exponentially with the atom number, as for N D-level atoms we have $\dim(\mathcal{H})=D^N$:

Two 2-level atoms $\rightarrow \dim(\mathcal{H}) = 4$

Three 3-level atoms $\rightarrow \dim(\mathcal{H}) = 27$

Four 4-level atoms $\rightarrow \dim(\mathcal{H}) = 256$.

Hence this makes numerical simulations difficult as well, since for solving the equations of motion via the master equation, the number of elements in the atomic density matrix is the respective dimension squared. By resorting to a Monte Carlo wavefunction simulation, one can get a quadratic reduction in the dimensions but the exponential increase of the Hilbert space will easily overshadow this performance improvement for say 8 atoms or more.
For our analytical treatment we are only considering three 3-level emitters, with 27 dimensions in $\mathcal{H}$ and investigate a special configuration of three atoms in an equilateral triangle, where the transition dipole unit vectors for each atom point inwards along the symmetry axis of the equilateral triangle and are orthogonal to the plane. The transition dipoles in each atom are mutually orthogonal as was explained in the section "Angular momentum conservation" and are shown in Fig.(3.1).

In Fig.(3.2) the V-type level scheme for identical atoms is shown with energy difference δ ($\hbar = 1$) between the excited levels.

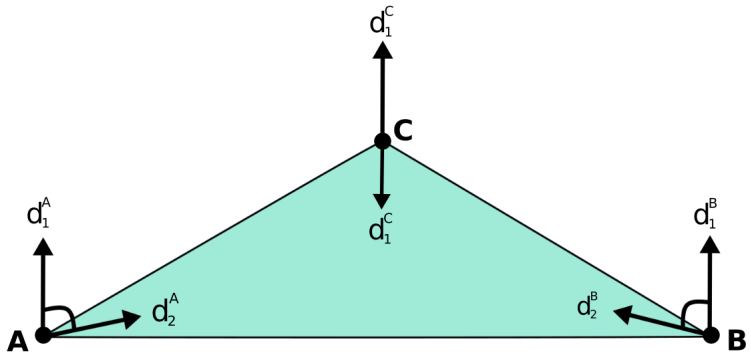

FIGURE 3.1: Equilateral triangle configuration for atoms A, B, C.

For the analytical as well as for the numerical treatment we assume identical atoms with degenerate atomic energy levels ω_0 ($\delta = 0$) and identical magnitudes of the transition dipole moments: $|\vec{\mu}_j^i| = \mu$, which amounts to a single atom spontaneos emission rate for each atom and transition of $\gamma = 4\omega_0^3\mu^2/3\hbar c^3$. [22]

With this setup we arrive at geometric parameters depending only on the relative coordinates between neighbouring atoms, and thus the combined interaction is composed of pairwise terms depending only on the distance between them and the transition dipole index j.

The geometric arrangement is shown in Fig.(3.3) with $\Gamma_j^{ii} = \gamma$ the single atom spontaneous emission rate, $k_0 = \omega_0/c = 2\pi/\lambda_0$ and $\Omega_j^{ii} = 0$.

3.2 Hamiltonian for an equilateral triangle

The Hamiltonian for this setup is given by

$$H = \omega_0 \sum_{j=1,2} \sum_{i}^{N=3} \sigma_j^{i+}\sigma_j^{i-} + \sum_{j=1,2} \sum_{i\neq k}^{N=3} \Omega_j \sigma_j^{i-}\sigma_j^{k+}, \tag{3.1}$$

and the Liouvillian reads:

$$\mathcal{L}[\rho_a] = \frac{1}{2} \sum_{ikj} \Gamma_j [2\sigma_j^{i-}\rho_a\sigma_j^{k+} - \sigma_j^{i+}\sigma_j^{k-}\rho_a - \rho_a\sigma_j^{i+}\sigma_j^{k-}], \tag{3.2}$$

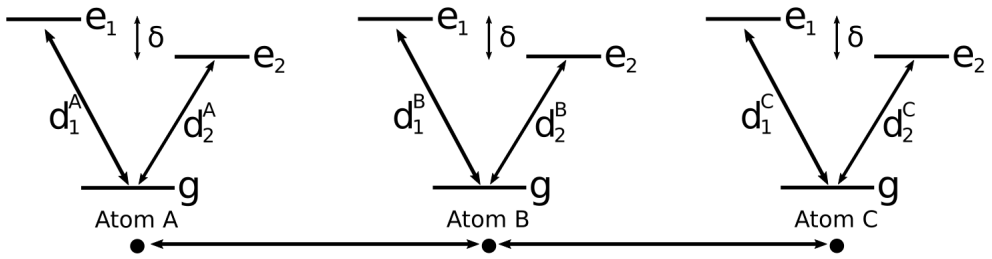

FIGURE 3.2: Illustration of three indentical V-type atoms A, B, C with nearly degenerate excited levels with $\delta \ll 1$.

where $\Omega_{jj'}^{ik} = \Gamma_{jj'}^{ik} = 0$ for $j \neq j'$, $\Omega_1 = \frac{3}{2}P_r(d), \Gamma_1 = \frac{3}{2}P_i(d), \Omega_2 = -\frac{3}{4}P_r(d) + \frac{9}{8}Q_r(d)$ and $\Gamma_2 = -\frac{3}{4}P_i(d) + \frac{9}{8}Q_i(d)$.

Here we have set:

$$P_r(r) = \frac{\cos r}{r} - \frac{\sin r}{r^2} - \frac{\cos r}{r^3}, P_i(r) = \frac{\sin r}{r} + \frac{\cos r}{r^2} - \frac{\sin r}{r^3}$$
$$Q_r(r) = \frac{\cos r}{r} - 3\frac{\sin r}{r^2} - 3\frac{\cos r}{r^3}, Q_i(r) = \frac{\sin r}{r} + 3\frac{\cos r}{r^2} - 3\frac{\sin r}{r^3}$$

In this case the superradiant state $|\psi_{sr}^3\rangle$ and the dark state $|\psi_d^3\rangle$ are eigenstates of the Hamiltonian with eigenenergies $E_{sr} = 2\omega_0 + \Omega_1 + \Omega_2, E_d = 2\omega_0 - \Omega_1 - \Omega_2$ respectively. Explicitly we have:

$$|\Psi_d^3\rangle = \frac{1}{\sqrt{3!}}\Big(|ge_1e_2\rangle + |e_1e_2g\rangle + |e_2ge_1\rangle - |ge_2e_1\rangle - |e_2e_1g\rangle - |e_1ge_2\rangle\Big) \tag{3.3}$$

and

$$|\Psi_{sr}^3\rangle = \frac{1}{\sqrt{3!}}\Big(|ge_1e_2\rangle + |e_1e_2g\rangle + |e_2ge_1\rangle + |ge_2e_1\rangle + |e_2e_1g\rangle + |e_1ge_2\rangle\Big) \tag{3.4}$$

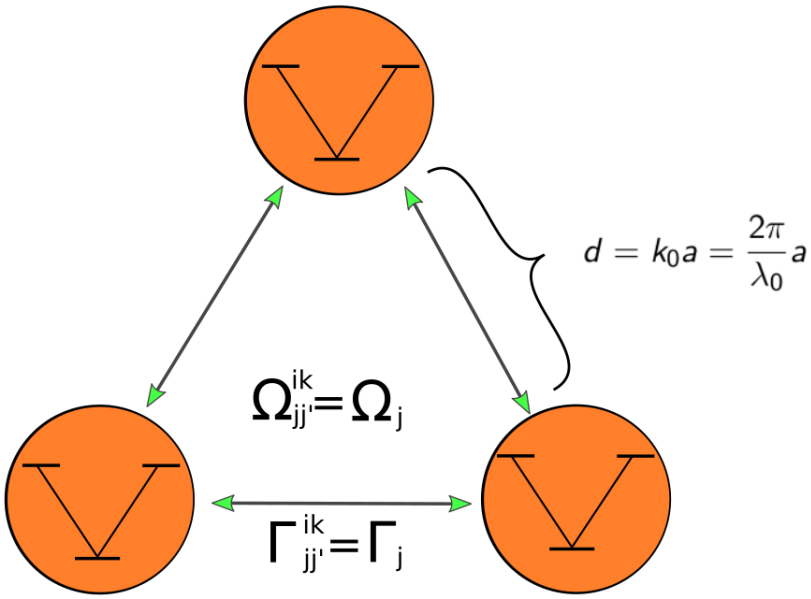

FIGURE 3.3: Equilateral triangle for three V-Systems.

By considering

$$\langle\psi|\mathcal{L}[|\psi_d^3\rangle\langle\psi_d^3|]|\psi\rangle \quad \text{and} \quad \langle\psi|\mathcal{L}[|\psi_{sr}^3\rangle\langle\psi_{sr}^3|]|\psi\rangle \tag{3.5}$$

where $|\psi\rangle$ are all the lower lying eigenstates into which the superradiant and subradiant state decays, we obtain the decay rates into the respective states. For $|\psi\rangle = |\psi_d^3\rangle$ or $|\psi\rangle = |\psi_{sr}^3\rangle$ we obtain the total decay rate.

Whereas for

$$\langle\psi_d^3|\mathcal{L}[|e_ie_je_k\rangle\langle e_ie_je_k|]|\psi_d^3\rangle \quad \text{and} \quad \langle\psi_{sr}^3|\mathcal{L}[|e_ie_je_k\rangle\langle e_ie_je_k|]|\psi_{sr}^3\rangle$$

where $i, j, k = 1, 2$ and $e_ie_je_k$ are the 8 possible inverted states which can feed the Super- and Subradiant states, we obtain the feeding rates (here γ refers to the spontanous emission rate from a single indipendent atom and is set to unity in numerical simulations):

TABLE 3.1: Feeding rates where the negative sign means that it gives the decay rate for the energetically higher lying state.

Feeding Rate from	$\|e_1e_1e_1\rangle$	$\|e_1e_1e_2\rangle$	$\|e_1e_2e_2\rangle$	$\|e_2e_2e_2\rangle$	$\|e_1e_2e_1\rangle$	$\|e_2e_2e_1\rangle$	$\|e_2e_1e_1\rangle$	$\|e_2e_1e_2\rangle$
for $\|\psi_d^3\rangle$	0	$-\frac{1}{3}\gamma+\frac{1}{3}\Gamma_1$	$-\frac{1}{3}\gamma+\frac{1}{3}\Gamma_2$	0	$-\frac{1}{3}\gamma+\frac{1}{3}\Gamma_1$	$-\frac{1}{3}\gamma+\frac{1}{3}\Gamma_2$	$-\frac{1}{3}\gamma+\frac{1}{3}\Gamma_1$	$-\frac{1}{3}\gamma+\frac{1}{3}\Gamma_2$
for $\|\psi_{sr}^3\rangle$	0	$-\frac{1}{3}\gamma-\frac{1}{3}\Gamma_1$	$-\frac{1}{3}\gamma-\frac{1}{3}\Gamma_2$	0	$-\frac{1}{3}\gamma-\frac{1}{3}\Gamma_1$	$-\frac{1}{3}\gamma-\frac{1}{3}\Gamma_2$	$-\frac{1}{3}\gamma-\frac{1}{3}\Gamma_1$	$-\frac{1}{3}\gamma-\frac{1}{3}\Gamma_2$

TABLE 3.2: Decay rates, where the first column is the total decay rate of the two states and the other columns are the decay rates to the lower lying eigentstates. The last column is the ground state.

$\|\psi_d^3\rangle$	$2\gamma-\Gamma_1-\Gamma_2$	0	0	$-\frac{1}{2}(\gamma-\Gamma_2)$	$-\frac{1}{2}(\gamma-\Gamma_1)$	$-\frac{1}{2}(\gamma-\Gamma_2)$	$-\frac{1}{2}(\gamma-\Gamma_1)$	0
$\|\psi_{sr}^3\rangle$	$2\gamma+\Gamma_1+\Gamma_2$	$-\frac{2}{3}\gamma-\frac{4}{3}\Gamma_1$	$-\frac{2}{3}\gamma-\frac{4}{3}\Gamma_2$	$-\frac{1}{6}\gamma+\frac{1}{6}\Gamma_2$	$-\frac{1}{6}\gamma+\frac{1}{6}\Gamma_1$	$-\frac{1}{6}\gamma+\frac{1}{6}\Gamma_2$	$-\frac{1}{6}\gamma+\frac{1}{6}\Gamma_1$	0

From the decay rate of the Dark State we see that in the limiting case of infinitely close atoms, the decay becomes even zero and the state is indeed stationary under the Liouvillian superoperator.

The same symmetry holds for the Λ-System as is discussed in [6]. It should be noted that for a three level ladder system the dark state does not exist anymore since the two transitions inside an atom are not indipendent.

3.2.1 Decay from a totally inverted state

If we diagonalize the Hamiltonian (3.1), two of the eigenstates are the subradiant and superradiant eigenstate, so called because there respective decay rates are $2\gamma-\Gamma_1-\Gamma_2$ and $2\gamma+\Gamma_1+\Gamma_2$ are really the most sub- and superradiant rates of all the eigenstates in the two excitation manifold. Of course the totally inverted states each have a decay rate of 3γ but as time progresses, the superradiance of $|\psi_{sr}^3\rangle$ dominates.
Unfortunately a perfectly dark state is not possible since the coupling terms at finite distance always lead to a slow decay even of $|\psi_d^3\rangle$, so the term "grey state" is coined. It still decays under the time evolution but of all intermediate states in the two excitation manifold it decays the slowest.

If we again consider the equation of motion for the atomic density operator

$$\frac{\partial\hat{\rho}_a}{\partial t}=i/\hbar[\hat{\rho}_a,\hat{H}]+\mathcal{L}[\hat{\rho}_a], \tag{3.6}$$

we see that if we look at the timeevolution of the eigenstates of the Hamiltonian, the commutator vanishes and we arrive at

$$\frac{\partial\hat{\rho}_{eig}}{\partial t}=\mathcal{L}[\hat{\rho}_{eig}]. \tag{3.7}$$

Upon projecting onto a target eigenstate we obtain the decay rate to this state. Finally by integration we obtain the time evolution of the respective eigenstate. [17]

$$\langle \hat{\rho}_{eig}(t) \rangle \propto \left(1 - e^{-\nu t}\right) e^{-\gamma t}, \tag{3.8}$$

ν denotes the feeding rate responsible for increasing the population and γ is the total decay rate of the state.
The time evolutions of the Sub- and Superradiant state for the initial state $|e_1 e_1 e_2\rangle$ are given by

$$\hat{\rho}_{dark}(t) = (1 - e^{\frac{1}{3}(-\Gamma+\gamma_1)t}) e^{-(2\Gamma-\gamma_1-\gamma_2)t}, \quad \hat{\rho}_{sr}(t) = (1 - e^{\frac{1}{3}(-\Gamma-\gamma_1)t}) e^{-(2\Gamma+\gamma_1+\gamma_2)t}$$

and time evolutions for the initial state $|e_1 e_2 e_2\rangle$

$$\hat{\rho}_{dark}(t) = (1 - e^{\frac{1}{3}(-\Gamma+\gamma_2)t}) e^{-(2\Gamma-\gamma_1-\gamma_2)t}, \quad \hat{\rho}_{sr}(t) = (1 - e^{\frac{1}{3}(-\Gamma-\gamma_2)t}) e^{-(2\Gamma+\gamma_1+\gamma_2)t}$$

and the decay rate for all 8 inverted states is:

$$\hat{\rho}_{inv}(t) = e^{-3\Gamma t}$$

.

In Fig.(3.4) the result of the analytical calculation of the time evolution is plotted [18] on a logarithmic scale. We see that the state $|\psi_d^3\rangle$ becomes dominant at late times.

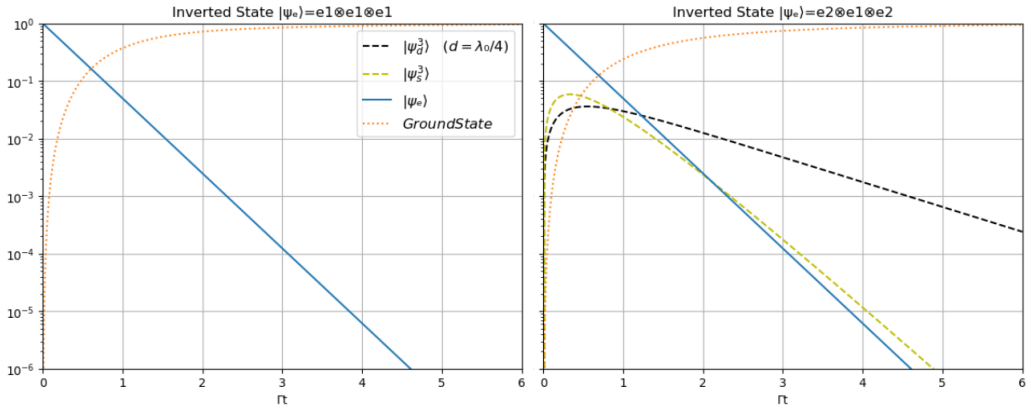

FIGURE 3.4: Decay of three V-type atoms in an equilateral triangle of size $d = \lambda_0/4$ starting at different totally inverted states. For the initial states $|e_1e_1e_1\rangle$ and $|e_2e_2e_2\rangle$ we see no excitations in the Super- and Subradiant states at all. The excited Population axis is scalled logarithmically (base 10) and the t axis is scaled with the single atom spont. emission rate Γ.

The decay channels starting from the totally inverted states via the Subradiant and Superradiant states are shown in Fig.(3.5) with their respective feeding and decay rates as well as their eigenenergies with the coherent energy shifts.

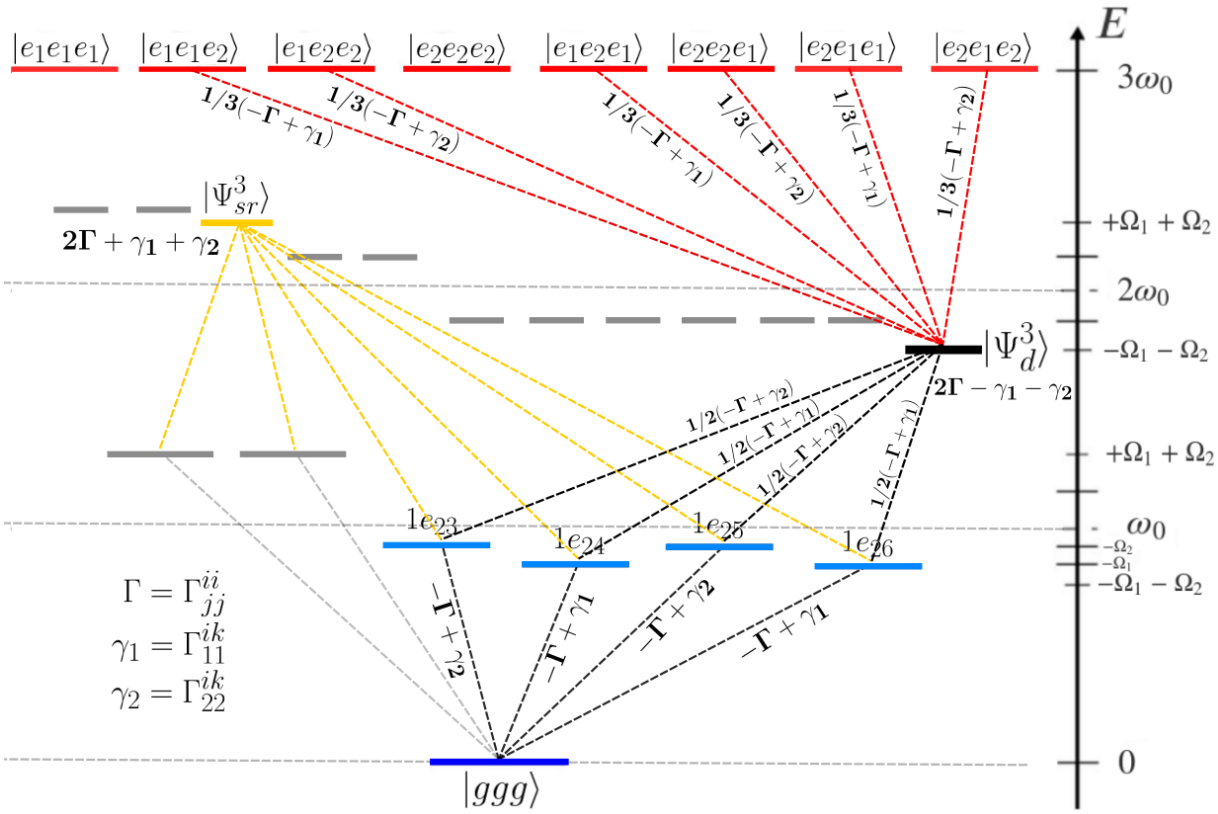

FIGURE 3.5: Level scheme for the Equilateral triangle of three V-type atoms. Decay channels with feeding- and decay-rates are only shown for the subradiant state for the sake of clarity and the feeding paths for the superradiant eigenstate are not shown.

In Fig. 3.5 we see, that as the atoms get closer together the decay rate of the dark state approaches zero, but at the same time, the feeding rate from energetically higher states also approach zero. Hence the dark state decouples from the electromagnetic vacuum and with it from eigenstates from the 3-excitation manifold.

3.2.2 Eigenstates and Eigenvalues

Now we calculate the Hamiltonian for the equilateral triangle configuration and calculate the eigenstates and their respective eigenenergies. In particular we show, that the super- and subradiant state are eigenstates of the system. The Hamiltonian

$$\hat{H} = \omega_0 \sum_{j=1,2} \sum_{i}^{N=3} \hat{\sigma}_j^{i+} \hat{\sigma}_j^{i-} + \Omega \sum_{j=1,2} \sum_{i \neq k}^{N=3} \hat{\sigma}_j^{i-} \hat{\sigma}_j^{k+} \tag{3.9}$$

lies in a 27 dimensional Hilbert space and has 8 totally inverted eigenstates with energy $3\omega_0$

$$\begin{aligned} &|e_1e_1e_1\rangle, |e_1e_1e_2\rangle, |e_1e_2e_2\rangle, |e_2e_2e_2\rangle, \\ &|e_1e_2e_1\rangle, |e_2e_2e_1\rangle, |e_2e_1e_1\rangle, |e_2e_1e_2\rangle \end{aligned} \tag{3.10}$$

Then there are 12 possibilities of product states with energy $2\omega_0$

$$\begin{aligned} &|e_1e_1g\rangle, |e_1ge_1\rangle, |ge_1e_1\rangle, |e_2e_2g\rangle, |e_2ge_2\rangle, |ge_2e_2\rangle, \\ &|e_1e_2g\rangle, |e_1ge_2\rangle, |ge_1e_2\rangle, |e_2e_1g\rangle, |e_2ge_1\rangle, |ge_2e_1\rangle, \end{aligned} \tag{3.11}$$

6 possibilities with energy ω_0

$$|e_1gg\rangle, |ge_1g\rangle, |gge_1\rangle, |e_2gg\rangle, |ge_2g\rangle, |gge_2\rangle, \tag{3.12}$$

and a single ground state

$$|ggg\rangle. \tag{3.13}$$

Here each collection of states constitutes a subspace which is orthogonal to the other subspaces, and therefore the eigenvalue equations can be solved for each collection independently.

For instance the eigenvalue equation for the single-excitation manifold leads to the following block-diagonal-matrix equation (The matrix is real and symmetric, therefore all eigenvectors can be choosen mutually orthogonal)

$$\begin{pmatrix} \begin{pmatrix} \omega_0 & \Omega_1 & \Omega_1 \\ \Omega_1 & \omega_0 & \Omega_1 \\ \Omega_1 & \Omega_1 & \omega_0 \end{pmatrix} & \\ & \begin{pmatrix} \omega_0 & \Omega_2 & \Omega_2 \\ \Omega_2 & \omega_0 & \Omega_2 \\ \Omega_2 & \Omega_2 & \omega_0 \end{pmatrix} \end{pmatrix} \begin{pmatrix} \alpha_1 \\ \alpha_2 \\ \alpha_3 \\ \alpha_4 \\ \alpha_5 \\ \alpha_6 \end{pmatrix} = \lambda \begin{pmatrix} \alpha_1 \\ \alpha_2 \\ \alpha_3 \\ \alpha_4 \\ \alpha_5 \\ \alpha_6 \end{pmatrix}$$

where for each block we get the following pairs of solutions (e.g. $(\alpha_1, \alpha_2, \alpha_3) = (\alpha_1, \alpha_2, \alpha_3, 0, 0, 0)$):

$(\alpha_1, \alpha_2, \alpha_3)$	Eigenvalue
(1,1,1)	$\omega_0 + \Omega_1 + \Omega_2$
(-1,1,0)	$\omega_0 - \Omega_1$
(1,1,-2)	$\omega_0 - \Omega_1$
$(\alpha_4, \alpha_5, \alpha_6)$	Eigenvalue
(1,1,1)	$\omega_0 + \Omega_1 + \Omega_2$
(-1,1,0)	$\omega_0 - \Omega_1$
(1,1,-2)	$\omega_0 - \Omega_2$

where the α's are the coefficients of the states in (3.12) and which give us the 6 normalized eigenstates and there corresponding eigenenergies with one excitation.

$$\underline{\omega_0 + \Omega_1 + \Omega_2 :} \begin{array}{l} |1e_{21}\rangle = \frac{1}{\sqrt{3}}(|e_1gg\rangle + |ge_1g\rangle + |gge_1\rangle) \\ |1e_{22}\rangle = \frac{1}{\sqrt{3}}(|e_2gg\rangle + |ge_2g\rangle + |gge_2\rangle) \end{array}$$

$$\underline{\omega_0 - \Omega_1 :} \begin{array}{l} |1e_{23}\rangle = \frac{1}{\sqrt{2}}(-|e_1gg\rangle + |ge_1g\rangle) \\ |1e_{25}\rangle = \frac{1}{\sqrt{6}}(|e_1gg\rangle - 2|gge_1\rangle + |ge_1g\rangle) \end{array}$$

$$\underline{\omega_0 - \Omega_2 :} \begin{array}{l} |1e_{24}\rangle = \frac{1}{\sqrt{2}}(-|e_2gg\rangle + |ge_2g\rangle) \\ |1e_{26}\rangle = \frac{1}{\sqrt{6}}(|e_2gg\rangle - 2|gge_2\rangle + |ge_2g\rangle) \end{array}$$

A analytical solution for the double excitation manifold is still doable, but the results are long and not claryfing, but still the super- and subradiant states retain their simple symmetric and antisymmetric form:

$$\underline{2\omega_0 + \Omega_1 + \Omega_2 :}\ |2e_{11}\rangle = \frac{1}{\sqrt{6}}(|e_1e_2g\rangle + |e_1ge_2\rangle + |ge_1e_2\rangle + |e_2e_1g\rangle + |e_2ge_1\rangle + |ge_2e_1\rangle)$$

$$\underline{2\omega_0 - \Omega_1 - \Omega_2 :}\ \boxed{|2e_{20}\rangle = \frac{1}{\sqrt{6}}(|e_1e_2g\rangle - |e_1ge_2\rangle + |ge_1e_2\rangle - |e_2e_1g\rangle + |e_2ge_1\rangle - |ge_2e_1\rangle)}$$

Although the dipole-dipole coupling coefficients are in general complicated expressions, for the equilateral triangle an analytical treatment was presented. In particular the energy level structure and the decay cascade for three three-level V-type emitters with its 27 eigenstates was analytically calculated and illustrated .

Chapter 4

Numerical Results

4.1 Linear Chain

In this section we are investigating a second simple geometry, namely a linear chain. Here due to more complex couplings we can only solve the master equation for the atomic density operator numerically. A conceptual scheme is shown in Fig.(4.1) where all transition dipole vectors are orthogonal to the interatomic distance vector and the dipole matrix elements are all real. The quantization axis is fixed along the interatomic distance vector connecting the atoms.

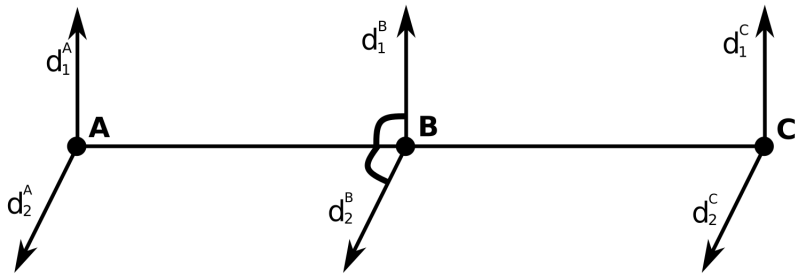

FIGURE 4.1: Linear Chain with parallel transition dipole moments.

Due to the rotation symmetry around the axis the dipole-dipole coupling coefficients become independent of the dipole index j and we obtain the following form of the Hamiltonian

$$\hat{H} = \omega_0 \sum_{j=1,2} \sum_{i}^{N=3} \hat{\sigma}_j^{i+} \hat{\sigma}_j^{i-} + \sum_{j=1,2} \sum_{i \neq k}^{N=3} \Omega^{ik} \hat{\sigma}_j^{i+} \hat{\sigma}_j^{k-} \tag{4.1}$$

Note that we still assume $\omega_1 = \omega_2 = \omega_0$ and $|\vec{\mu_j^i}| = \mu$. The dissipative coupling coefficient in the Liouvillian becomes independent of the j index as well:

$$\mathcal{L}[\hat{\rho}] = \frac{1}{2}\sum_{ikj}\Gamma^{ik}[2\hat{\sigma}_j^{i-}\hat{\rho}\hat{\sigma}_j^{k+} - \hat{\sigma}_j^{i+}\hat{\sigma}_j^{k-}\hat{\rho} - \hat{\rho}\hat{\sigma}_j^{i+}\hat{\sigma}_j^{k-}] \tag{4.2}$$

where $\Omega_{jj'}^{ik} = \Gamma_{jj'}^{ik} = 0$ for $j \neq j'$ and $\Gamma_{jj}^{ik} = \Gamma^{ik}$.

The coefficient matrix for the coherent energy shifts and decay rates are as follows

$$\Omega_1^{ik} = \Omega_2^{ik} := \begin{pmatrix} 0 & \Omega_1 & \Omega_2 \\ \Omega_1 & 0 & \Omega_1 \\ \Omega_2 & \Omega_1 & 0 \end{pmatrix}, \Omega_1 = \Omega(r), \Omega_2 = \Omega(2r), \Omega(r) = \frac{3}{2}P_r(r), r = \frac{\lambda_0}{12}, \gamma_0 := 1$$

$$\Gamma_1^{ik} = \Gamma_2^{ik} := \begin{pmatrix} 1 & \Gamma_1 & \Gamma_2 \\ \Gamma_1 & 1 & \Gamma_1 \\ \Gamma_2 & \Gamma_1 & 1 \end{pmatrix}, \Gamma_1 = \Gamma(r), \Gamma_2 = \Gamma(2r), \Gamma(r) = \frac{3}{2}P_i(r)$$

with $\Gamma = 1$ and where P_r and P_i are given by

$$P_r(r) = \frac{\cos r}{r} - \frac{\sin r}{r^2} - \frac{\cos r}{r^3}, P_i(r) = \frac{\sin r}{r} + \frac{\cos r}{r^2} - \frac{\sin r}{r^3}$$

For this particular configuration the two most subradiant eigenstates are given by

$$|\psi_{subr,2}\rangle = \frac{1}{2}(|e_1e_2g\rangle - |ge_1e_2 - e_2e_1g\rangle + |ge_2e_1\rangle), \quad E_1 = 2\omega_0 + \Omega_2$$

$$|\psi_{subr,1}\rangle = \frac{1}{\mathcal{N}}(-|e_1e_2g\rangle + c\cdot|e_1ge_2\rangle - |ge_1e_2\rangle + |e_2e_1g\rangle - c\cdot|e_2ge_1\rangle + |ge_2e_1\rangle),$$

$$E_2 = 2\omega_0 - \frac{\Omega_2}{2} - \frac{\sqrt{\Omega_2^2 + 8\Omega_1^2}}{2},$$

where $\mathcal{N} = \sqrt{4 + 2c^2}$, $c = \frac{\Omega_1\left(3\Omega_2 + \sqrt{\Omega_2^2+8\Omega_1^2}\right)}{\Omega_2^2+2\Omega_1^2+\Omega_2\sqrt{\Omega_2^2+8\Omega_1^2}}$

and e_1e_2g means $e_1 \otimes e_2 \otimes g$ with $e_1 = (1,0,0)^T, e_2 = (0,1,0)^T, g = (0,0,1)^T$ in the computational(standard) basis.

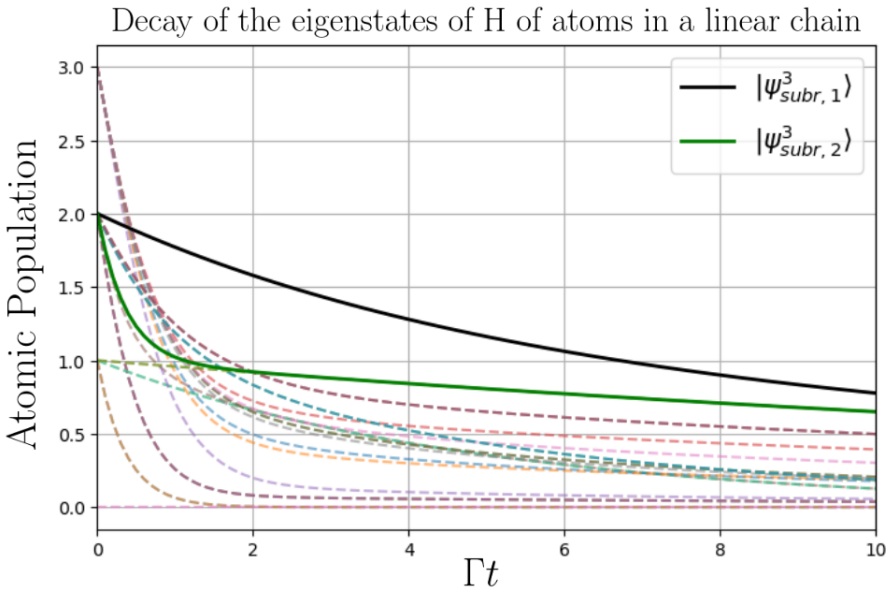

FIGURE 4.2: Numerical Simulation: Upper state occupation decay of the 27 eigenstates of H for three V-type atoms in a linear chain of distance $d = \lambda_0/12$. The two most subradiant states with two excitations are highlighted and in the limit of $\Omega_1 = \Omega_2$ the state $|\psi^3_{subr,1}\rangle$ becomes $|\psi^3_d\rangle$.

In the case when $\Omega_1 = \Omega_2 := \Omega$, which is only atainable for the equilateral triangle, it follows that $c = 1$ and $\mathcal{N} = \sqrt{6}$, therefore: $|\psi_{subr,1}\rangle = |\psi^3_d\rangle$ with $E = 2\omega_0 - 2\Omega$

The decay of all 27 eigenstates are plotted in Fig.(4.2), where the two states considered above are highlighted and indeed show the most subradiance. It should be noted that there are also subradiant states in the one excitation manifold which show the same behaviour at later times, but with a lower atomic population.
Finally in Fig. 4.3 we plot the decay of different states in the linear chain. Although the Dark State is not an eigenstate of the Hamiltonian in this configuration, we show it to highlight its subradiant character, along with other states.

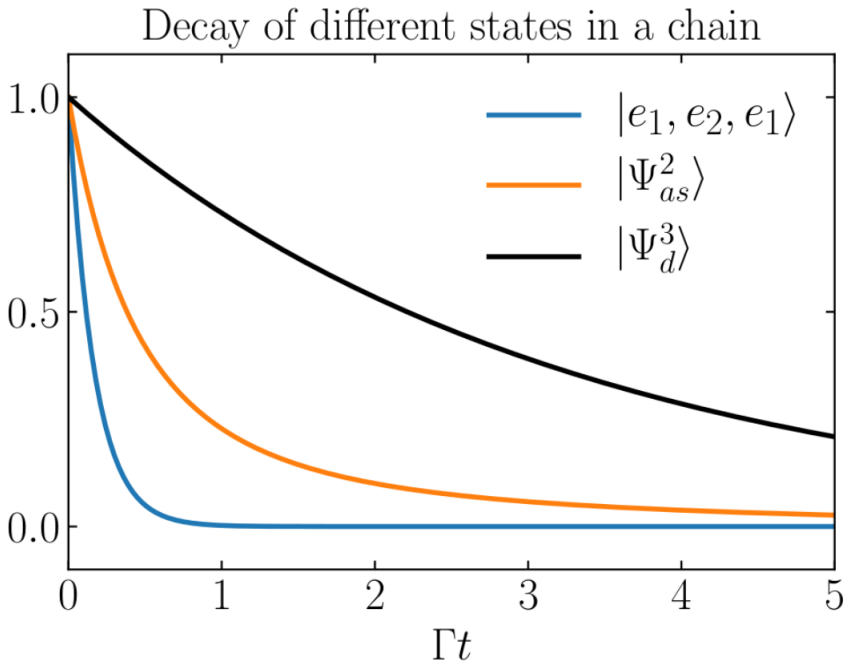

FIGURE 4.3: The decay for various states is shown, where $|\Psi^2_{as}\rangle = 1/\sqrt{2}(|e_1e_2\rangle - |e_2e_1\rangle)|g\rangle$

4.1.1 Overlap with the Dark State

As we have seen in the previous section, for arbitrary geometric configurations, the most dark and superradiant (symmetric) state are not eigenstates of the Hamiltonian, but it is still the case that the eigenstates which have the largest overlap with $|\Psi^3_d\rangle$ also show the most subradiance. Therefore we investigate this property for different transition dipole orientations in the linear chain, since this value somewhat indicates the subradiant behaviour of the whole geometric configuration, the appropriate one could be chosen quickly.

So for instance in Fig. 4.4 (C) the following dipole orientations in spherical coordinates are chosen

$$\vec{\mu^i_1} = (0,0,1)^T, \quad \vec{\mu^3_2} = (1,0,0)^T \tag{4.3}$$
$$\vec{\mu^1_2} = (\cos\varphi_1, \sin\varphi_1, 0)^T, \quad \vec{\mu^2_2} = (\cos\varphi_2, \sin\varphi_2, 0)^T.$$

In Fig.4.4(A) the ϑ angles vary for the outside dipoles in z direction, whereas in (B) all three dipoles are held parallel and rotate in all spherical directions simultaneously.

The color gradient indicates the degree of overlap with the perfect dark state $|\psi_d^3\rangle$ and brightest areas having the most overlap of close to unity.

In order to create the plots, the angles are varied in discrete steps over the whole intervall of either 0 to 2π for φ or 0 to π for θ and for each orientation the eigenstates are caclulated and the value of $Max\{\langle\psi_d^3|\psi_{eig}\rangle\}$ is plotted.

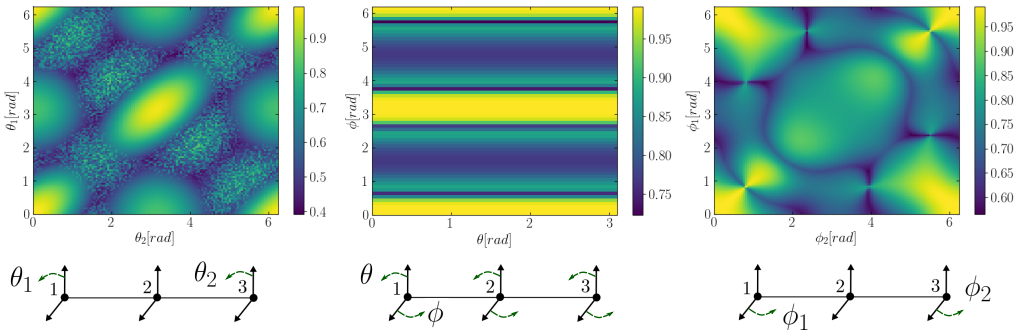

FIGURE 4.4: Plots of the overlap with the dark state for different configurations at distance $d = \lambda_0/4$. In the first plot on the left only θ angles for atom 1 and 2 are rotated. In the middle figure all dipoles are kept parallel by simultaneous rotation and it can be seen that for each ϕ-angle the overlap is constant along θ. Although the maximal overlap of one is only reached for the equilateral triangle, it is almost one.

Finally in Fig. 4.5 the interatomic distances are varied for the linear chain and the decay rates for the most subradiant and superradiant state in the two-excitation manifold are plotted, since $|\Psi_d^3\rangle$ and $|\Psi_{sr}^3\rangle$ also reside in this manifold. In the special case of the symmetric triangle configuration, these can be identified with $|\Psi_d^3\rangle$ and $|\Psi_{sr}^3\rangle$. Here r_1 and r_2 correspond to the seperation between atom 1 and 2 and atom 2 and 3 respectively.

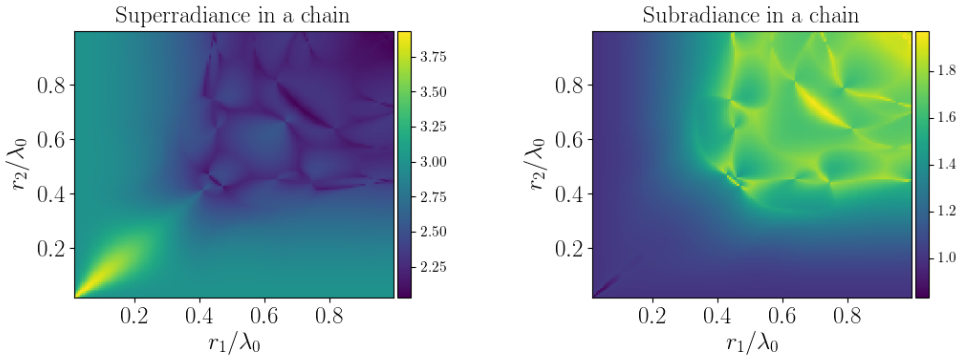

FIGURE 4.5: *Contour plot of the decay rates of the most superradiant and subradiant states in the two-excitation manifold for different interatomic seperations. Note that the theoretic maximum and minimum decay rate is* 4γ *and* 0 *respectively.*

4.2 Triangular atomic array

For a numerical simulation of the equilateral triangle [19] we assume the geometry as shown in Fig.(3.1), where again the dipole-dipole coupling coefficients assume the form $\Gamma_{jj}(d)$ and $\Omega_{jj}(d)$. That means, the coefficients are independent of the atomic indices since the transition dipole orientations are along the symmetry axes of the equilateral triangle. Additionally one transtion in each atom is orthogonal to the plane spanned by the triangle, therefore the cross coupling terms vanish i.e. $\Gamma_{jj'} = \Omega_{jj'} = 0$ for $j \neq j'$.
The decay of the Sub- and Superradiant eigenstate are plotted in Fig.(4.6) as well as the independent decay, that is for the limiting case where the interatomic distance goes to infinity i.e. $\Gamma_{jj}^{ik} = \delta_{ik}$, where $\gamma = 1$ for simplicity.

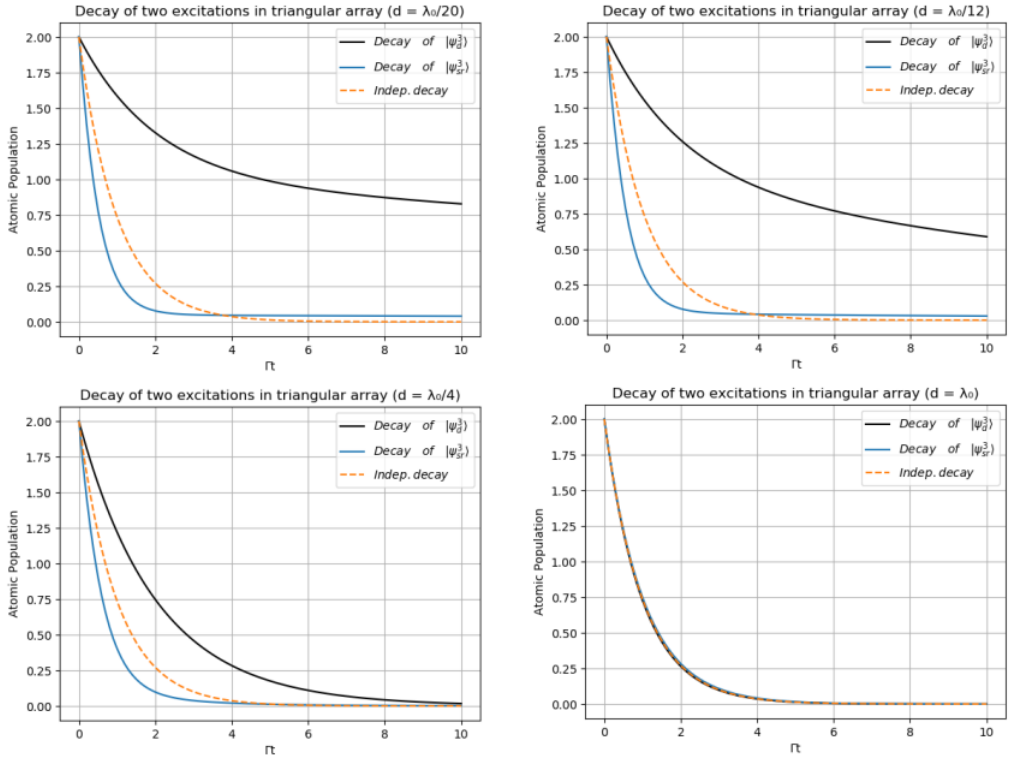

FIGURE 4.6: Upper state population decay of three interacting V-type atoms in an equilateral triangle of different sizes. As the size increases all decay rates become identical. The black line corresponds to the dark state decay, whereas the blue line to the superradiant decay. Here the interatomic distance is denoted by d.

As was mentioned in chapter 2 the dark state can be seen as the Laplace-Expansion along the first row of the determinant of the following matrix, with tensor instead of scalar multiplication:

$$\begin{vmatrix} e_1 & e_2 & g \\ e_1 & e_2 & g \\ e_1 & e_2 & g \end{vmatrix}$$

where the subdeterminants are given by

$$|\psi_{unp,1}\rangle = \frac{1}{\sqrt{2}}|g\rangle \otimes \big(|e_1\rangle \otimes |e_2\rangle - |e_2\rangle \otimes |e_1\rangle\big)$$

$$|\psi_{unp,2}\rangle = \frac{1}{\sqrt{2}}|e_2\rangle \otimes \big(|e_1\rangle \otimes |g\rangle - |g\rangle \otimes |e_1\rangle\big)$$
$$|\psi_{unp,3}\rangle = \frac{1}{\sqrt{2}}|e_1\rangle \otimes \big(|e_2\rangle \otimes |g\rangle - |g\rangle \otimes |e_2\rangle\big)$$

and are unpolarized product states involving all three atomic states, meaing the first atom is uncorrelated with the superposition of the other two atoms.

Here the dark state can also be written as follows:

$$|\psi_d^3\rangle = \frac{1}{\sqrt{3}}\Big(|\psi_{unp,1}\rangle + |\psi_{unp,2}\rangle + |\psi_{unp,3}\rangle\Big)$$

In Fig.(4.7) the three unpolarized product states as well as the Sub- and Superradiant states are plotted at a finite distance of $d = \lambda_0/12$. It can be seen that the unpolarized states clearly show subradiance as well, with the Dark State decaying the slowest as it is the sum of all three unpolarized product states and results in a maximally entangled state involving all three atoms simultaneously.

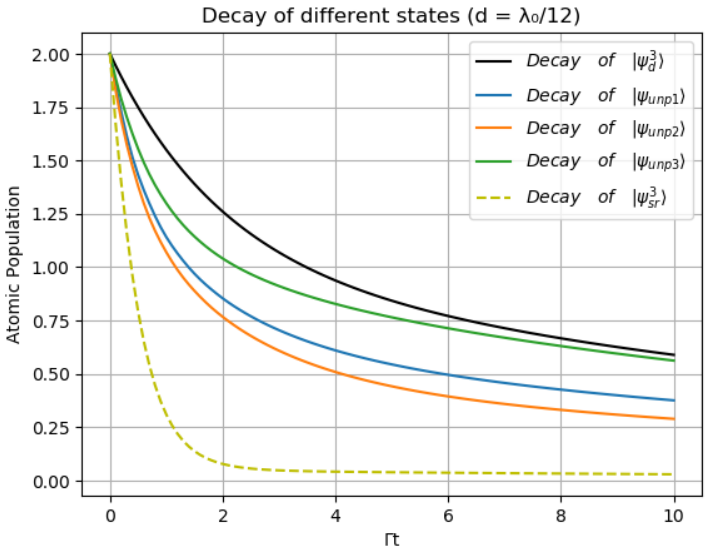

FIGURE 4.7: Population decay for three closely spaced V-type atoms for different doubly excited initial states in an equilateral triangle configuration of size $d = \lambda_0/12$. Here Γ refers to the spontanous emission rate of a single atom.

Now we allow for non-degeneracy between the excited energy levels and plot the decay of different scenarious in Fig. 4.8.

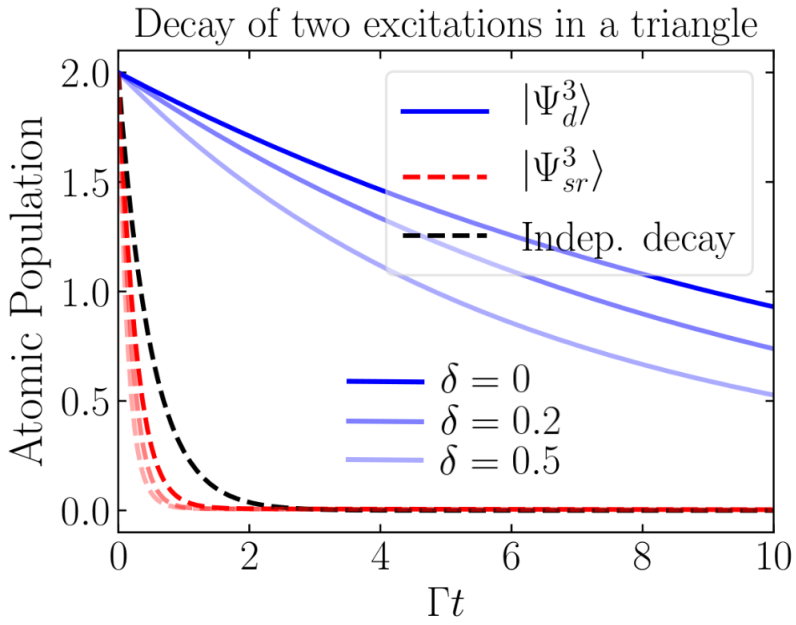

FIGURE 4.8: Decay of the Superadiant- and Dark-State, as well as the independent case where all three atoms decay individually. Here $\omega_1 - \omega_2 = \delta$ with $\omega_1 = 1$ for the numerics and the atomic seperation is $\lambda_0/12$.

4.2.1 Dark state overlap

Now we look at different dipole orientations and again use the overlap with the dark state $|\psi_d^3\rangle$ to look for geometries that favor subradiant behaviour.

In Fig.(**??**) two dipoles rotated by discrete steps via φ in the intervall $[0, 2\pi]$, and the configuration that represents the symmetric case, which is treated in chapter 3 analytically is highlighted in the plot.

In Fig.(**??**) we see poor subradiant behaviour, as the the dipole ortientations don't align with the symmetry axes of the triangle and except for $\theta = 0, \pi/2, \pi$ the dipole-dipole cross coupling terms are non-zero and induce additional collective decay between the atoms.

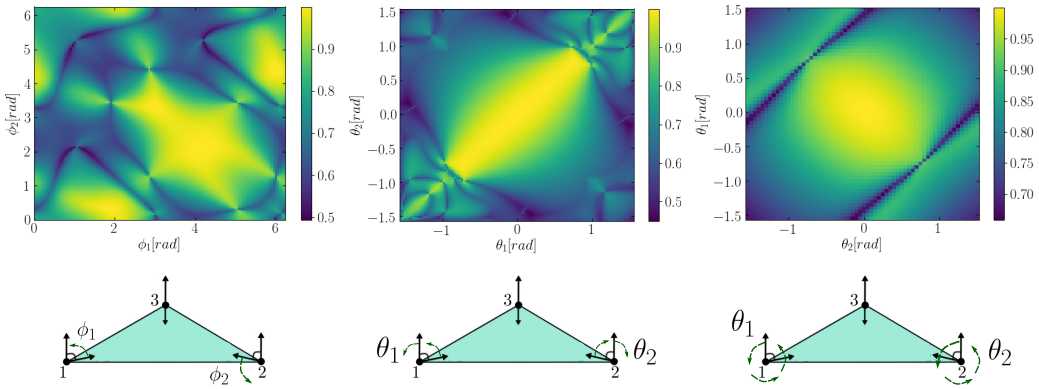

FIGURE 4.9: Equilateral triangle configuration at $d = \lambda_0/4$ with various rotations of the dipoles. In the first plot on the left the ϕ angles in spherical coordinates are rotated where for $\phi_2 = 2\pi/3$ and $\phi_1 = 4\pi/3$ the maximum overlap of unity is obtained. The maximum overlap for the other figures is $(\theta_1, \theta_2) = (0, 0)$ where for the last plot only the first transitions in atom 1 and 2 are varied.

Chapter 5

Dissipative Preparation of Dark States

5.1 Decay from higher excited states for larger atom numbers $N \geq 3$

As is shown and discussed in [3] for Λ-type systems, a simple method to prepare the dark state probabilistically, is to use the singlet Bell state of two atoms together with the third atom in the ground state as the initial state. Let us first study this idea here too for the equilateral triangle. In Fig. (5.1) the numerical simulation of the decay for 3 atoms in a equilateral triangle is shown, with the inital state $|\Psi_{Bell}\rangle \otimes |g\rangle$, where $|\Psi_{Bell}\rangle = \frac{1}{\sqrt{2}}(|e_1, e_2\rangle - |e_2, e_1\rangle)$. It can be seen, that the inital probability for the Dark State $|\Psi_d^3\rangle$ is $\approx 1/3$.

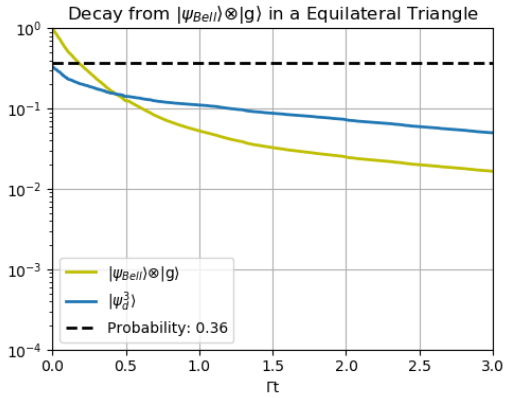

FIGURE 5.1: Logarithmic plot of the probabilities during decay of 3 atoms in a equilateral triangle at distance $d = \lambda_0/4$. The probabilities for $|\Psi_{Bell}\rangle \otimes |g\rangle$ and $|\Psi_d^3\rangle$ are shown.

It can be seen, that $|\Psi_{Bell}\rangle \otimes |g\rangle$ has a large overlap with $|\Psi_d^3\rangle$. This leads to a favorable dissipative preperation probability for the dark state and we will now investigate this behaviour for larger atom numbers.

Let us now look at 4 atoms and choose a tetrahedral configuration as shown in Fig. (5.2). Atom 1 and 2 are initially in the singlet state and Atom 3 and 4 prepared in the ground state. There are 4 possible dark states of the equilteral triangle type, which are connected to the 4 faces of the tetrahedron, but for the probability we only consider the two dark states for which Atom 1 and 2 are involved namely $|\Psi_d^3\rangle \otimes |g\rangle$ and the dark state where Atom 3 is in $|g\rangle$, as these configurations are the most favorable ones as is discussed above and is shown numerically in Fig.(5.3). A time adapted Monte Carlo wave function method is used for the numerical simulations. The discrete time steps are set such that most of them are taken in the beginning of the dissipative process, where the dynamics of the system are maximal, assuming no external driving field such as a laser is involved.

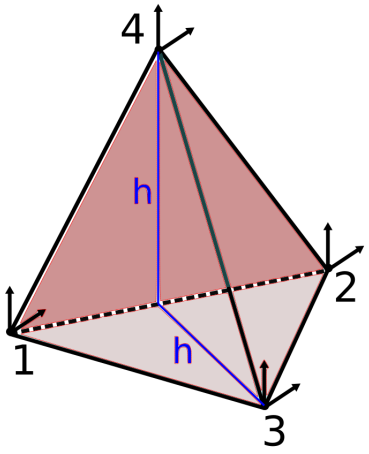

FIGURE 5.2: 4 Atoms in a Tetrahedra (Pyramid) with side-length a and $h = \frac{\sqrt{3}a}{2}$

.

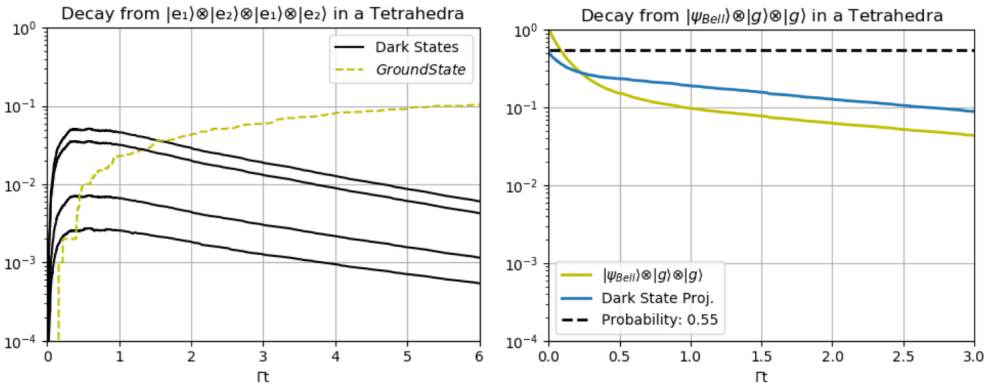

FIGURE 5.3: On the left the probability for the four possible dark states decay of a totally inverted state $|e_1, e_2, e_1, e_2\rangle$ is shown with the probability for the four possible dark states. On the right the decay with initially atoms 1 and 2 entangled and atoms 3 and 4 in the ground state, as well as the probability for the ending up in the dark state with atoms 1,2,3 or atoms 1,2,4 involved.

In Fig.(5.4) the situation is depicted when a fifth atom is added. With the initial probability for being in one of the 3 dark states as shown in the picture is initially $\approx 60\%$ due to its large overlap with the three possible dark states.

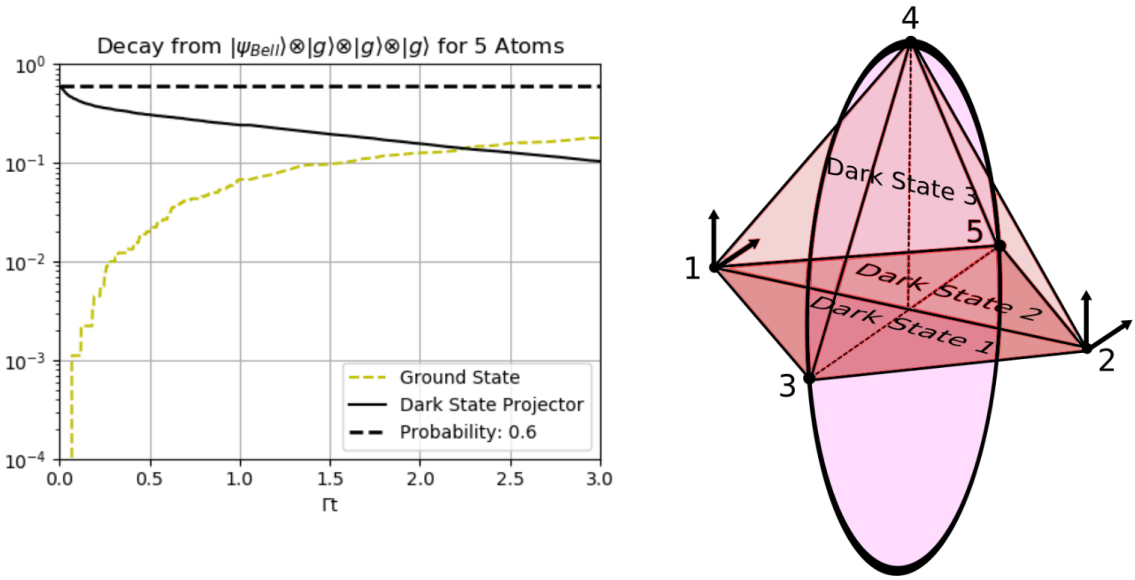

FIGURE 5.4: 5 Atoms with the inital state $|\Psi_{Bell}\rangle \otimes |g, g, g\rangle$. A circle of radius h is shown (the height of the equilateral triangle) on which the atoms initially in the ground state are positioned. Error bars in the Monte Carlo simulation are excluded as we only want to illustrate the trend of increasing subradiance with atom number.

5.2 Larger atom numbers

The idea is to increase the number of atoms on the circle of radius h, which are initially in the ground state, with Atoms 1 and 2 in the entangled singlet state. As a final simulation in Fig.(5.5) a configuration with 6 Atoms and 10 Atoms is shown, where the initial ground state atoms are equally spaced around the circle. For 10 atoms it can be seen, that the inital probability for the atoms to be in one of the 8 dark states is ≈ 0.8.

As the dimension of the Hilbert space for 10 3-level atoms is 3^{10}, the numerical simulation was carried out via a Monte Carlo wave function method to first order with sparse matrices and adapted time intervals, which is discussed in more detail in the appendix.

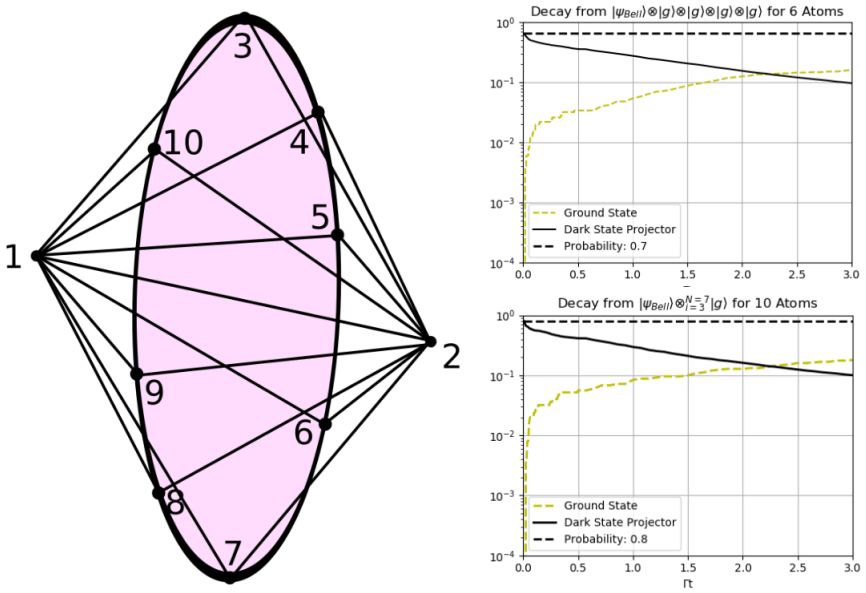

FIGURE 5.5: On the left the configuration with 10 atoms is shown, where Atom 1 and 2 are in the entangled singlet state and on the right the two Monte Carlo simulations of the decay with 6 and 10 atoms respectively. The error bars in the Monte Carlo calculations are neglected, as these plots should only illustrate the trend of increasing subradiance.

5.3 Preparation by optical pumping

Now let us add a driving laser by adding $\hat{H}_l = \sum_{i,j} \eta(\hat{\sigma}_j^i + \hat{\sigma}_j^{i\dagger})$ to the Hamiltonian, to look for other methods of dark state preparation. Hence the atoms are continously excited and decay. One can hope, that atomic population accumulates in those states which have the slowest decay. In Fig. 5.6 we plot look at the linear chain with four 4-level atoms and compare the survival probabilities for a driving laser versus no driving laser.

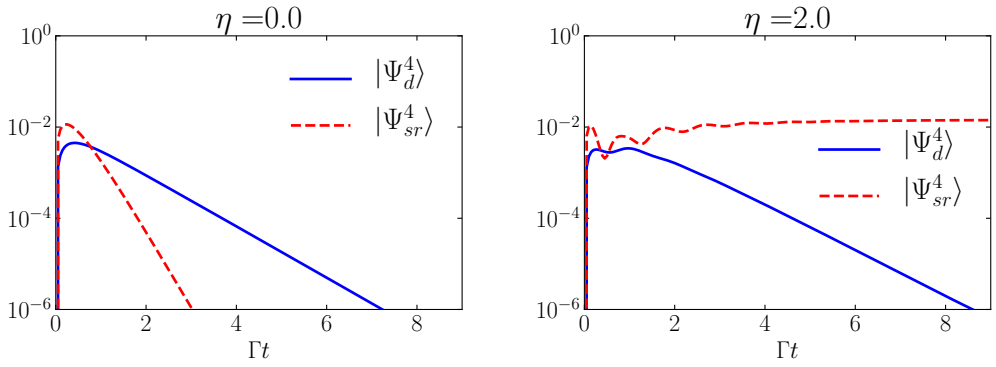

FIGURE 5.6: *Survival probability in a linear chain of four 4-level atoms with* $d = \lambda_0/12$ *seperation and with the initial state* $|e_1, e_1, e_2, e_3\rangle$.

Finally in Fig. 5.7 we look at the probabilities to prepare $|\Psi_d^3\rangle$ and $|\Psi_{sr}^3\rangle$ by optical pumping starting from the ground state $|ggg\rangle$. In the contour plot of Fig. 5.7 we see that for interatomic distances $\approx \lambda_0/100$ the dark state starts to decouple from the driving laser as the feeding rates approach zero. Note that for optimal parameters the preparation probability approaches a maximum value of around 2.5%.

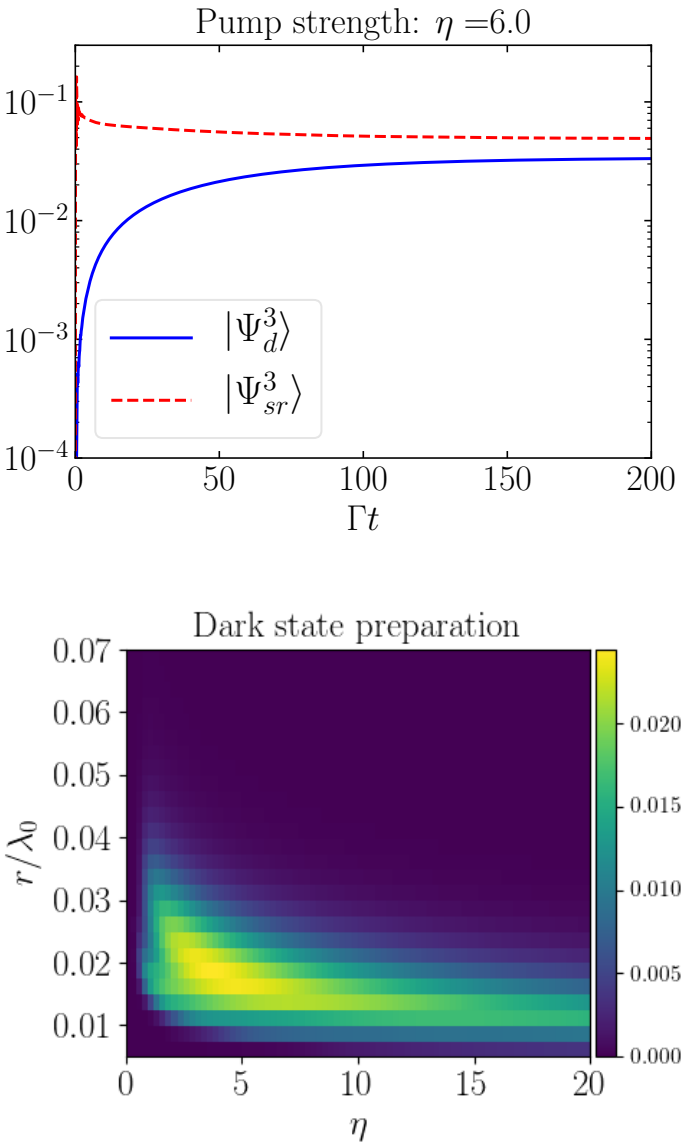

FIGURE 5.7: *(Left) Preparation probability for the Dark- and Symmetric-State at* $r = \lambda_0/50$ *in a linear chain. (Right) Preparation probabilities for different atomic separations and pumping strengths in a linear chain after* $\Gamma t = 200$.

Chapter 6

Conclusions

We have analyzed the collective decay of closely spaced identical V-type atoms with orthgonal transitions and the atoms having closely lying excited energy levels. We derive a corresponding Hamiltonian using the dipole approximation. Eliminating the EM vacuum modes, the equations of motion were derived for the atomic density operator within the Markov-Born approximation.
The obtained master equation was than applied to three identical V-type systems in a equilateral triangle configuration and in a linear chain model, where the interatomic seperations are only a fraction of the resonant wavelength λ_0. After having introduced the concept of subradiance, we found that only for the equilateral triangle with one of the two transition dipole vectors orientied along the reflection-symmetric axis of the triangle and the other orthogonal to the plane spanned by the triangle, the dark state is an eigenstate of the Hamiltonian. For all other orientations and geometries considered this is not the case, but still many subradiant states exist in the N-1 down to 1 excitation manifolds for N atoms with N-1 indepedent transitions. For $N = 3$ we have shown that these subradiant states show a large overlap with the dark state $|\psi_d^3\rangle$ and in the limiting case of infinitely close atoms, become perfectly dark.
By choosing orthogonal dipole matrix elements and orienting one transition dipole vector per atom orthogonal to the interatomic distance vector, it is possible to eliminate the dipole-dipole cross coupling coefficients and maximize the subradiance, which becomes particularly apparent when the decay of $|\psi_{sr}^3\rangle$ and $|\psi_d^3\rangle$ is compared. It is shown, that the super- and subradiance become much more pronounced when $d \ll \lambda_0$ and approach each other for $d \approx \lambda_0$ in terms of decay behaviour.
For future consierations, a generalization to V-type system with more atoms could be considered with more interesting geometries, eventhough the dissipative preparation probability of the dark state will be very small under this conditions, the sub- and superradiance of the whole system could still be analyzed especially by considering atoms with degrees of freedom in spacial coordinates, since even cold clouds of atoms are accompanied by vibrations around the atomic center of mass.

In summary, it can be concluded that the theoretical and numerical investigation of collective subradiance of generic atomic arrays plays an important part in real world applications like the storage of quantum information, the improvement of coherence times in optical atomic clocks or the preparation of entanglement resources for quantum cryptography.

Chapter 7

Appendix A: Derivation of $\chi^{ik}_{jj'}(\omega_0)$

The following presents the essential steps for deriving $\chi^{ik}_{jj'}(\omega_0)$, where we follow closely [17] and [20]. We saw in Chapter 2, that the polarization sum has the following resolution:

$$\sum_{\lambda}(\vec{\mu_i}\cdot\vec{\epsilon}_{k,\lambda})(\vec{\mu_k}\cdot\vec{\epsilon}_{k,\lambda}) = \mu^2\Big[e_{\mu_i}\cdot e_{\mu_k} - (e_{\mu_i}\cdot e_{\vec{k}})(e_{\mu_k}\cdot e_{\vec{k}})\Big] \tag{7.1}$$

where e_x denotes the unit vector in direction x.

The next step was to replace the summation with an integration over the continuum of modes by

$$\sum_{k,\lambda} \to \frac{V}{(2\pi)^3}\int_{\Omega_k} d^3k = \frac{V}{(2\pi)^3}\int\int k^3 d\Omega_k dk sin\ \theta_k \tag{7.2}$$

in the expressions for $\Omega^{ik}_{jj'}$ and $\Gamma^{ik}_{jj'}$.

This results in integrals of the form

$$\int_0^\infty dk \int_\Omega d\Omega_k \Big(\pi\delta(k_0-k)+\frac{1}{k_0-k}-\frac{1}{k_0+k}\Big)\Big(e_{\mu_i}\cdot e_{\mu_k}-(e_{\mu_i}\cdot e_{\vec{k}})(e_{\mu_k}\cdot e_{\vec{k}})\Big)e^{i\vec{k}\cdot\vec{r}_{ik}} \tag{7.3}$$

where we substituted $\omega_0 = ck_0$ and $\omega_k = ck$.

We calculate the solid angle part first by

$$\int_\Omega d\Omega_k e^{i\vec{k}\cdot\vec{r}_{ik}} = \frac{4\pi sin\ kr_{ik}}{kr_{ik}}. \tag{7.4}$$

with $\vec{k}\cdot\vec{r}_{ik} = kr_{ik}cos\ \theta_k$, $d\Omega_k = d\theta_k sin\ \theta_k d\varphi_k$ and the substitution $x = cos\ \theta_k$. Then we proceed with the polarization part in the integrand:

$$\Big(e_{\mu_i}\cdot e_{\mu_k} - (e_{\mu_i}\cdot e_{\vec{k}})(e_{\mu_k}\cdot e_{\vec{k}})\Big) \tag{7.5}$$

where

$$(e_{\mu_i}\cdot e_{\vec{k}})(e_{\mu_k}\cdot e_{\vec{k}}) = \frac{(e_{\mu_i}\cdot\nabla_r)(e_{\mu_k}\cdot\nabla_r)}{k^2} = \tag{7.6}$$

$$\frac{(e_{\mu_i}\cdot\nabla_r)(e_{\mu_k}\cdot e_r\partial_r)}{k^2} = \frac{(e_{\mu_i}\cdot\nabla_r)(cos\ \theta_{\mu_k}\partial_r)}{k^2} =$$

$$\frac{(e_{\mu_i}\cdot(e_r\partial_r + e_\theta\frac{1}{r}\partial_\theta)(cos\ \theta_{\mu_k}\partial_r)}{k^2} = cos\ \theta_{\mu_i}cos\ \theta_{\mu_k}\partial_r^2 - \frac{sin\ \theta_{\mu_i}sin\ \theta_{\mu_k}}{r}\partial_r =$$

$$cos\ \theta_{\mu_i}cos\ \theta_{\mu_k}\partial_r^2 + \frac{e_{\mu_i}\cdot e_{\mu_k}}{r}\partial_r - \frac{cos\ \theta_{\mu_i}cos\ \theta_{\mu_k}}{r}\partial_r,$$

with $cos\ (\theta_{\mu_i} - \theta_{\mu_k}) = e_{\mu_i}\cdot e_{\mu_k}$ and $cos\ \theta_{\mu_i} = e_{\mu_i}\cdot e_k$, as can be deduced from Fig.(2.5).

Now if we apply this to the solid angle part and carry out the calculation we arrive at

$$F(\xi) = \frac{3}{2}\Bigg[\Big(e_{\mu_i}\cdot e_{\mu_k} - (e_{\mu_i}\cdot e_{r_{ik}})(e_{\mu_k}\cdot e_{r_{ik}})\Big)\frac{sin\ \xi}{\xi} \tag{7.7}$$

$$+\Big(e_{\mu_i}\cdot e_{\mu_k} - 3(e_{\mu_i}\cdot e_{r_{ik}})(e_{\mu_k}\cdot e_{r_{ik}})\Big)\Big(\frac{cos\ \xi}{\xi^2} - \frac{sin\ \xi}{\xi^3}\Big)\Bigg]$$

with $\xi = kr_{ik}$.

The integral in Eq.(7.3) is now of the form

$$\int_0^\infty d\xi\pi\delta(\xi_0-\xi)F(\xi)\xi^3 - \int_{-\infty}^\infty d\xi\xi^3\frac{F(\xi)}{\xi-\xi_0} \tag{7.8}$$

where we used the fact that

$$\int_0^\infty d\xi\frac{F(\xi)}{\xi+\xi_0} = \int_{-\infty}^0 d\xi\xi^3\frac{F(\xi)}{\xi-\xi_0}. \tag{7.9}$$

Now we use a result from complex analysis which states that the closed loop integral of a holomorphic function $F(z)$ can be expressed as

$$\lim_{\eta\to 0}\oint dz\frac{F(z)}{z-z_0+i\eta} = -i\pi F(z_0) + P\int_{-\infty}^\infty\frac{F(z)}{z-z_0}dz, \tag{7.10}$$

and by comparing this with the expressions for $\Gamma^{ik}_{jj'}$ and $\Omega^{ik}_{jj'}$, we deduce that the imaginary part of the loop integral corresponds to $\Gamma^{ik}_{jj'}$ and the real part to $\Omega^{ik}_{jj'}$. Therefore we proceed to calculate the loop integral by taking the contour as show in Fig.(7.1) and expression the cosine and sine as complex exponentials and adding $i\epsilon_{\to 0}$ in the denominator to displace the singularity ξ_0:

$$\Omega^{ik}_{jj'} = \frac{1}{\xi_0^3} \lim_{\epsilon \to 0} Re \left\{ \oint \frac{d\xi}{2\pi} \frac{F(\xi)}{\xi - \xi_0 - i\epsilon} \right\}, \tag{7.11}$$

$$\Gamma^{ik}_{jj'} = \frac{1}{\xi_0^3} \lim_{\epsilon \to 0} Im \left\{ \oint \frac{d\xi}{2\pi} \frac{F(\xi)}{\xi - \xi_0 - i\epsilon} \right\}, \tag{7.12}$$

where

$$\chi^{ik}_{jj'}(\omega_0) = \frac{1}{\xi_0^3} \lim_{\epsilon \to 0} \oint \frac{d\xi}{2\pi} \frac{F(\xi)}{\xi - \xi_0 - i\epsilon}, \tag{7.13}$$

with the i, k, j, j' dependence absorbed in ξ and $F(\xi)$.
After taking the contour and applying the residuum theorem to the loop which encloses the singularity we arrive at $\chi^{ik}_{jj'}(\omega_0)$.

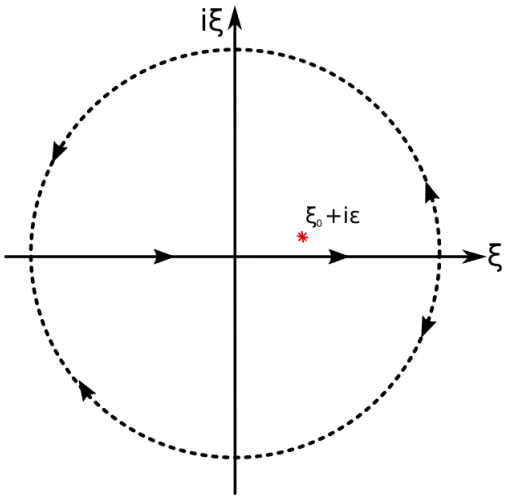

FIGURE 7.1: Contour integral, where the integration on the real line is taken once, and for the upper semi-circle the residuum theorem is applied.

Chapter 8

Appendix B: Monte Carlo wave-function method

In order to obtain the quantum jump operators for our dissipative system, we first diagonalize the coefficient matrix $\Gamma^{ik}_{jj'}$ in the master equation and consequently write

$$\dot{\rho} = -\frac{i}{\hbar}\big[H,\rho\big] + \sum_i \big(J_i\rho J_i^\dagger - \frac{1}{2}J_i^\dagger J_i\rho - \frac{1}{2}\rho J_i^\dagger J_i\big) \tag{8.1}$$

where the $J_i = \sum_k c_i\sigma_k$ is a linear combination of the transition dipole operators and c_i is the ith eigenvalue of $\Gamma^{ik}_{jj'}$.

The coherent time evolution is calculated according to a Schroedinger equation with a non-hermitian Hamiltonian $H_{nH} = H - \frac{i\hbar}{2}\sum_i J_i^\dagger J_i$

$$i\hbar\frac{\mathrm{d}}{\mathrm{d}t}|\Psi(t)\rangle = H_{\mathrm{nH}}|\Psi(t)\rangle. \tag{8.2}$$

Now we Taylor expand the solution only up to first order in time, which is a farly good approximation as long as the time steps are kept small.

$$|\Psi(t+dt)\rangle = \Big(1 - \frac{iH_{nH}dt}{\hbar}\Big)|\Psi(t)\rangle. \tag{8.3}$$

The matrix representations of all the operators and state vectors turn out to be very sparse, so for instance for 4 atoms the matrix of a dipole transition operator of a particular atom and transition has only 27 non-zero entries but 6534 zero entries, therefore sparse vectors/matrices are used throughout the calculations.

As was mentioned, the Hamiltonian is non-hermitian and so the norm of the state is not conserved, and decreases over time. This is easy to see, since for longer time intervals the total Jump rate in this time interval grows and consequently decreases H_{nH}.

The jump rates in a particular time step are given by

$$\delta p_m = dt\langle\Psi(t)|J_m^\dagger J_m|\Psi(t)\rangle \tag{8.4}$$

and the total jump rate by $\delta p = \sum_m \delta p_m$. This follows from the deviation of the norm of $|\Psi(t+dt)\rangle$:

$$\langle\Psi(t+dt)||\Psi(t+dt)\rangle = 1 - \delta p \tag{8.5}$$

We require that $\delta p \ll 1$ in order that the probability for two or more jumps occuring in the same timestep is negligible, since the time evolution is only to first order where single quantum jumps are considered.
For a quantum jump to occur in a given time step we choose a random number τ between 0 and 1 and look for a M such that

$$\frac{1}{\delta p}\sum_{m=0}^{M-1} p_m < \tau < \frac{1}{\delta p}\sum_{m=0}^{M} p_m \tag{8.6}$$

If such a M exists a quantum jump occurs according to

$$|\Psi(t+dt)\rangle = \sqrt{dt}\frac{J_m|\Psi(t)\rangle}{\sqrt{\delta p_m}} \tag{8.7}$$

and otherwise no jump occurs and the state follows the linearized non-hermitian evolution derived from the Schroedinger equation above.

For choosing the time steps, it turns out that equal time steps are not the most efficient way, and with adapted time steps the dynamics of the system can be simulated much more accurately. In general there are adaptive methods as in [21], but for the dissipative system considered here the dynamics are much more predictable and it suffices to set the time intervals a priori, according to the criterion that $\delta p \ll 1$ at any given time step. Or in other words, if the jump rates are changing fast and therefore the system is changing fast, smaller time steps are necessary to capture the dynamics, and if the jump rates are small the system's change is small and larger time steps are sufficient.
In Fig(8.1) a plot is shown for the dissipation of three atoms in a equilateral triangle, where with equidistant time steps we see that the greatest rate of change occurs in the first 1/5 of the time evolution, so it is sensible to allocate most of the timesteps into this time interval, as is shown on the right side of Fig.(8.1). This leads to further improvement in the numerical simulation, since less time steps are needed to achieve a good approximation.

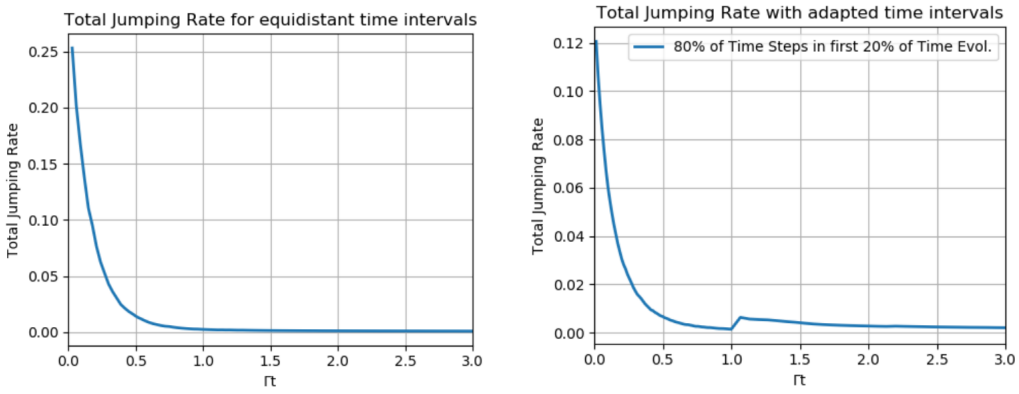

FIGURE 8.1: Plot of the total jump rate times the time step: δpdt over the time evolution, where on the right side most time steps are taken at the very beginning of the dissipative process.

Bibliography

[1] Subradiance in a Large Cloud of Cold Atoms, William Guerin, Michelle O. Araújo, and Robin Kaiser *Phys. Rev. Lett. 116, 083601 (2016)*

[2] Dicke, Robert H. (1954). "Coherence in Spontaneous Radiation Processes". Physical Review. 93 (1): 99–110

[3] Walls, D. F.; Gerard J. Milburn (1994). "Quantum Optics"

[4] Crispin Gardiner, Peter Zoller, "The Quantum World of Ultra-Cold Atoms and Light Book II: The Physics of Quantum-Optical Devices" (2015)

[5] M. O. Scully, "Single Photon Subradiance: Quantum Control of Spontaneous Emission and Ultrafast Readout," Phys. Rev. Lett. 115, 243602 (2015).

[6] M. Hebenstreit, B. Kraus, L. Ostermann, H. Ritsch, Phys. Rev. Lett. 118, 143602 (2017)

[7] Breuer, Heinz-Peter; F Petruccione (2002). "The theory of open quantum systems".

[8] Ahsan Nazir, Heather Carmichael, "Lecture notes on open quantum systems" (2012)

[9] Bartelmann M., Feuerbacher B., Krüger T., Lüst D., Rebhan A., Wipf A., "Theoretische Physik" (2015)

[10] G. M. Moy, J. J. Hope, and C. M. Savage, Born and Markov approximations for atom lasers, Phys. Rev. A 59, 667 - 675 (1999)

[11] Ahsan Nazir, Heather Carmichael, "Lecture notes on open quantum systems" (2012)

[12] Lemberg, R.H. "Radiation from an N-Atom system. i. general formalism". Phys. Rev. A2, 883–888 (1970).

[13] Lemberg, R.H. "Radiation from an N-Atom System. II. Spontaneous Emission from a Pair of Atoms". Phys. Rev. A 2, 889 (1970).

[14] Michael A. Nielsen and Isaac L. Chuang. Quantum Computation and Quantum Information. 10th Anniversary Edition. Cambridge University Press, 2010.

[15] J. I. de Vicente, C. Spee, and B. Kraus, Physical Review Letters 111, 110502 (2013).

[16] Supplemental Material of Phys. Rev. Lett. 118, 143602 (2017)

[17] L. Ostermann, "Collective Radiation of Coupled Atomic Dipoles and the Precise Measurement of Time" (2016)

[18] J. D. Hunter. "Matplotlib: A 2D graphics environment". In:Computing In Science Engineering 9.3 (2007), pp. 90–95. doi:10.1109/MCSE.2007.55

[19] Rackauckas, C. Nie, Q., (2017). DifferentialEquations.jl – A Performant and Feature-Rich Ecosystem for Solving Differential Equations in Julia. Journal of Open Research Software. 5(1), p.15. DOI: http://doi.org/10.5334/jors.151

[20] G.S. Agarwal, Anil K. Patnaik, Phys. Rev. A 63, 043805 (2001)

[21] Kornyik, M Vukics, András. (2019). The Monte Carlo wave-function method: A robust adaptive algorithm and a study in convergence. Computer Physics Communications. 10.1016/j.cpc.2018.12.015.

[22] Z. Ficek, R. Tanas, S. Kielich, Physica 146A (1987) 452-482

[23] Agarwal G 2012 Quantum Optics (Cambridge: Cambridge University Press)

universität innsbruck

Eidesstattliche Erklärung

Ich erkläre hiermit an Eides statt durch meine eigenhändige Unterschrift, dass ich die vorliegende Arbeit selbständig verfasst und keine anderen als die angegebenen Quellen und Hilfsmittel verwendet habe. Alle Stellen, die wörtlich oder inhaltlich den angegebenen Quellen entnommen wurden, sind als solche kenntlich gemacht.

Die vorliegende Arbeit wurde bisher in gleicher oder ähnlicher Form noch nicht als Magister-/Master-/Diplomarbeit/Dissertation eingereicht.

24.01.2019

Datum

Unterschrift